

Infrared Photometric Analysis of White Dwarfs from The Two Micron All Sky Survey and the Spitzer Space Telescope

P.-E. Tremblay and P. Bergeron

*Département de Physique, Université de Montréal, C.P. 6128, Succ. Centre-Ville,
Montréal, Québec, Canada, H3C 3J7.*

tremblay@astro.umontreal.ca, bergeron@astro.umontreal.ca

ABSTRACT

We review the available near- and mid-infrared photometry for white dwarfs obtained from the Two Micron All-Sky Survey (2MASS) and by the *Spitzer Space Telescope*. Both data sets have recently been used to seek white dwarfs with infrared excesses due to the presence of unresolved companions or circumstellar disks, and also to derive the atmospheric parameters of cool white dwarfs. We first attempt to evaluate the reliability of the 2MASS photometry by comparing it with an independent set of published *JHK* CIT magnitudes for 160 cool white dwarf stars, and also by comparing the data with the predictions of detailed model atmosphere calculations. The possibility of using 2MASS to identify unresolved M dwarf companions or circumstellar disks is then discussed. We also revisit the analysis of 46 binary candidates from Wachter et al. using the synthetic flux method and confirm the large near-infrared excesses in most objects. We perform a similar analysis by fitting *Spitzer* 4.5 and 8 μm photometric observations of white dwarfs with our grid of model atmospheres, and demonstrate the reliability of both the *Spitzer* data and the theoretical calculations up to 8 μm . Finally, we search for massive disks resulting from the merger of two white dwarfs in a 2MASS sample composed of 57 massive degenerates, and show that massive disks are uncommon in such stars.

Subject headings: binaries: general – infrared: stars – planetary systems: proto-planetary disks – stars: fundamental parameters – white dwarfs

1. INTRODUCTION

With the recent All-Sky Data Release of the Two Micron All-Sky Survey¹ (2MASS), we are now able to retrieve near-infrared (NIR) J , H , and K_S magnitudes for more than a thousand white dwarfs that fall within the 2MASS detection limit. This database was used in several studies aimed at identifying new cool white dwarfs (e.g., de La Fuente Marcos et al. 2005) or circumstellar disks (Kilic et al. 2006a) and seeking binary candidates (Wachter et al. 2003; Holberg et al. 2005; Debes et al. 2005). In the latter case, one of the main interests are the binary systems containing a main sequence star and a white dwarf. These systems might reveal important details about stellar populations and evolution. Different techniques have been used to seek these binary candidates. Until recently, most systematic searches were based on surveys of resolved common proper-motion binaries (Silvestri et al. 2002), but new interest has emerged for identifying unresolved binaries. One of the reasons is that accretion from a previously unknown close companion could account for the high metal abundances observed in some white dwarfs. The preferred method for seeking unresolved binary candidates is to perform a photometric analysis. In the case where the companion is an M dwarf, the white dwarf star usually dominates the observed flux in the optical regions. Therefore, it is natural to look for an excess in the NIR, either photometrically or spectroscopically, where the contribution from the M dwarf becomes dominant (see Dobbie et al. 2005, for a review).

Exploiting the 2MASS photometric data, different methods of analysis were used to identify NIR excesses. Wachter et al. (2003) used the second incremental 2MASS data release, which covers about 50% of the sky. The authors took the approach of a ($J-H$, $H-K_S$) two-color diagram for 795 white dwarfs recovered from the 2MASS survey. They identified 95 binary candidates, including 47 objects with prior evidence of binarity. They also suggested 15 additional tentative binary candidates. Wellhouse et al. (2005) used a similar two-color diagram approach with a sample of 51 magnetic white dwarfs as candidates for potential pre-cataclysmic variables. While they did not find any binary candidates, they identified 10 objects with peculiar colors associated with very low mass companions or debris. Holberg et al. (2005) used the final 2MASS All-Sky Data Release to study the 347 DA stars from the Palomar-Green Survey (Liebert et al. 2005). Their technique relies on the spectroscopic determinations of effective temperature and surface gravity, which combined with the observed V magnitude, can be used to compare magnitudes predicted at J , H , and K_S with those available in the 2MASS Point-Source Catalog (PSC). The same technique had been used before by Zuckerman & Becklin (1992) and Green et al. (2000) but with in-

¹See <http://www.ipac.caltech.edu/2mass/releases/allsky/>

dependent NIR photometric data sets. The disadvantage of this technique is that reliable atmospheric parameters and V magnitudes must be available for each star.

As the low-mass main-sequence companion gets cooler — typical of late-type M or L dwarfs — only a mild NIR excess is observed. The NIR excesses expected from circumstellar dust disks and planets around white dwarfs could be even less significant. Zuckerman & Becklin (1987) were the first to identify such a system for the $0.7 M_{\odot}$ DAZ star G29-38 (2326+049), also a ZZ Ceti pulsator. More recently, Kilic et al. (2005) and Becklin et al. (2005) went through a detailed analysis of GD 362 (1729+371), a massive DAZ star with unusually high metal abundances, some nearly solar (Gianninas et al. 2004). For both objects, there was a small but significant excess in the NIR that could be detected in the K band. However, it is from the large mid-infrared (MIR) excess (Reach et al. 2005; Becklin et al. 2005) that the disks could be confirmed. NIR spectroscopic observations and 2MASS data have also been used by Kilic et al. (2006a) to identify a third DAZ white dwarf, GD 56, that could harbor a circumstellar disk, although this object has yet to be observed in the MIR. Chary et al. (1999) and Kilic et al. (2005, 2006a) analyzed a dozen other DA and DAZ stars and found no evidence for similar circumstellar disks. Jura (2003) discussed possible scenarios and concluded that not all white dwarfs with heavy elements in their atmospheres possess a dust disk similar to that of G29-38. The current picture is that as much as 14% of the DAZ stars host a circumstellar disk (Kilic et al. 2006a).

According to Livio et al. (2005), disks and planets could also result from the merger of two white dwarfs. Hence, the high-mass tail of the white dwarf mass distribution (see, e.g., Liebert et al. 2005) would represent the most promising candidates to search for such disks or planets. Livio et al. suggest that a typical dust disk would have a mass and radius of $M_d \sim 0.007 M_{\odot}$ and $R_d \sim 1$ AU, respectively. This is much larger and massive than the disk proposed for G29-38 (Jura 2003). Therefore, the predicted flux excess should be easily detected in the NIR (assuming a standard composition and geometry) and the 2MASS survey should provide a useful tool to further constrain the proposed model.

In addition to the 2MASS NIR photometry, there is a developing interest to observe white dwarfs at longer wavelengths in the MIR. The *Spitzer Space Telescope* IRAC² photometry and IRS infrared spectroscopy have been used in recent surveys of relatively bright, nearby white dwarfs to better constrain the atmospheric parameters of cool white dwarfs (Kilic et al. 2006b) and to seek MIR excesses from disks (Reach et al. 2005; Hansen et al. 2006). Since the contribution of a cold disk becomes dominant only in the MIR, the *Spitzer* data set is more sensitive to search for disks than the NIR 2MASS data set.

²See <http://ssc.spitzer.caltech.edu/irac/>

Before undertaking a more systematic search of white dwarf stars in binaries or of circumstellar disk systems using 2MASS or *Spitzer* data, it seems appropriate as a first step to evaluate properly the reliability of the infrared photometric data sets and the ability of current model atmospheres to reproduce the observations. We thus present in § 2 a comparison of 2MASS photometry with published *JHK* magnitudes on the CIT photometric system for 160 cool white dwarfs, and assess the limitations of the 2MASS survey. We then evaluate in § 3 the usefulness of the 2MASS photometric data for identifying binary candidates using various techniques, and discuss the implications of our results on several studies published in the literature. In § 4, we perform a similar analysis but using the *Spitzer* IRAC 4.5 and 8 μm photometry presented in Kilic et al. (2006b). Finally in § 5, we analyze a sample of 57 white dwarfs with spectroscopic masses above $0.8 M_{\odot}$ together with 2MASS photometry to search for disks around massive white dwarfs, such as those predicted by Livio et al. (2005). Our conclusions follow in § 6.

2. COMPARISON OF CIT AND 2MASS PHOTOMETRY

Our photometric sample used to compare against the 2MASS data is drawn from the detailed photometric and spectroscopic analyses of Bergeron et al. (1997, hereafter BRL97), Leggett et al. (1998), and Bergeron et al. (2001, hereafter BLR01) who obtained improved atmospheric parameters of cool white dwarfs from a comparison of optical *BVRI* and infrared *JHK* photometry with the predictions of model atmospheres appropriate for these stars. We selected from these studies 183 cool white dwarfs with infrared *JHK* magnitudes measured on the CIT photometric system (with the exception of 0704–508 that has no *K* measurement). This sample covers a range of effective temperatures between $T_{\text{eff}} \sim 4000$ K and 13,000 K, and all objects have been successfully fitted by BRL97 and BLR01 under the assumption of single stars (or double degenerates) with no evidence for any infrared excess that could be due to the presence of an unresolved low-mass main sequence star.

We searched the 2MASS PSC for all white dwarfs in our sample using the GATOR batch file tool and a $20''$ search window centered on a set of improved coordinates measured by J. B. Holberg (2005, private communication). In most instances, multiple sources were found within the search window and we unambiguously identified each object by comparing the 2MASS atlas with the finding charts available from the online version of the Villanova White Dwarf Catalog³. We recovered the 2MASS *J*, *H*, and *K_S* magnitudes for 160 stars from our initial CIT photometric sample of 183 objects. The remaining 23 objects were dropped from

³<http://www.astronomy.villanova.edu/WDCatalog/index.html>

our analysis for the following reasons: 9 were too faint for the 2MASS survey, 11 were not properly resolved due to the presence of a nearby star, and 3 could not be unambiguously identified from the comparison of the 2MASS atlas and the published finding charts. Our final sample of 160 cool white dwarfs is presented in Table 1 where we provide the CIT and 2MASS magnitudes for each object. The uncertainties of the CIT magnitudes are 5% except where noted in Table 1, and the 2MASS photometric uncertainties are given in parentheses (magnitudes with null uncertainties represent lower limits).

Since the two data sets rely on completely different photometric systems, we must keep in mind that there could be a possible offset between both systems. For instance, Carpenter (2001) have obtained an empirical color transformation (see their eqs. 12 to 15) based on a comparison of CIT and 2MASS photometry for 41 stars. However, since this transformation has been obtained in a broad general context and not specifically for cool white dwarfs, we first compare directly both photometric data sets without any transformation, and discuss the possible offsets in the present context.

Figure 1 shows the differences in magnitudes between the infrared CIT and 2MASS photometric systems for the J , H , and K/K_S filters for the white dwarfs from Table 1. Note that the number of stars in each panel is different (159 in J , 157 in H , and 143 in K_S) since some stars have not been formally detected in one or more bands, and only lower limits are available. The size of the error bars in Figure 1 correspond to the combined quadratic uncertainties of both data sets, $\sigma = (\sigma_{2\text{MASS}}^2 + \sigma_{\text{CIT}}^2)^{1/2}$. For both measurements to be compatible, the error bar must touch the horizontal dashed line in each panel of Figure 1, which represents the mean magnitude difference between both data sets, as determined below.

We present in Table 2 a statistical comparison of both data sets for all three bands. The first three lines correspond to the full data set while the last three lines are restricted to 2MASS magnitudes that satisfy the level 1 requirements. The second column indicates the number of stars used for the comparison (to be included, the 2MASS magnitude must have a measurement error). The third and fourth columns represent respectively the mean and the standard deviation of the magnitude differences for each band. These mean values thus correspond to the zero point offsets between both photometric systems, and we therefore adopt the following transformation based on the most accurate subsample (level 1): $J_{\text{CIT}} = J_{2\text{MASS}} - 0.0083$, $H_{\text{CIT}} = H_{2\text{MASS}} + 0.0094$ and $K_{\text{CIT}} = K_{S\ 2\text{MASS}} + 0.0133$. We note that the offsets are typically five times smaller than the average 2MASS uncertainties — given in the fifth column of Table 2, $\langle\sigma_{2\text{MASS}}\rangle$ — and these could as well be considered as zero for most practical purposes. We also note that since the effective wavelength of the 2MASS K_S filter (2.169 μm) is slightly shorter than that of the CIT K filter (2.216 μm), the observed flux

should be larger at K_S than at K , and a larger *positive* offset is thus expected for this band, as is indeed observed in Table 2.

If the uncertainties of both data sets have been properly evaluated, the average combined quadratic uncertainties, $\langle\sigma\rangle$ (last column of Table 2), should be at least as large as the standard deviations of the magnitude differences (fourth column of Table 2). This is certainly the case for the level 1 subsample, a result that confirms the reliability of the 2MASS level 1 photometry. For the complete sample, however, the $\langle\sigma\rangle$ values are slightly below the standard deviations. If we assume that the CIT photometric uncertainties have been properly estimated, which is supported in BRL97 and BLR01 by the successful fits with white dwarf models, the 2MASS uncertainties might be slightly underestimated in the case of faint cool white dwarfs near the survey limit. Another way of interpreting these results is to note that in Figure 1, the magnitudes are not compatible within the 1σ combined uncertainties for 34.6%, 30.6%, and 35.0% of the stars in the complete sample at the J , H and K bands, respectively. These correspond to the objects whose error bars do not cross the horizontal dashed lines. This occurs for level 1 and fainter objects as well. At a 3σ level, these numbers drop to 0.6%, 1.9% and 4.2%, respectively, which suggest that there are infrequent but large discrepancies at K_S .

In Figure 2, we compare $(J - H, H - K/K_S)$ two-color diagrams for various data sets. In the upper panels, we compare the two-color diagrams for the 143 stars in common in both the CIT and the 2MASS samples that have been detected by 2MASS in all three bands. The 2MASS colors appear much more scattered than the CIT colors, and this simply reflects the larger uncertainties of the former data set. Indeed, if we restrict the sample to the 49 objects that satisfy the level 1 requirements, the scatter of the 2MASS diagram is greatly reduced, as shown in the bottom panels of Figure 2. For this restricted sample, both CIT and 2MASS data appear to have a similar scatter, which is a confirmation of the comparable mean uncertainties. Since the 2MASS photometry has been used to infer the presence of unresolved white dwarf and low mass main sequence binaries, one needs to be cautious when interpreting data sets that include objects below the level 1 requirements.

For instance, we indicated by open circles in Figures 1 and 2 ten objects whose optical $BVRI$ and infrared JHK photometry on the CIT system has been successfully fitted with single white dwarf models by BRL97 and BLR01. They cover a range in 2MASS J magnitudes from 13.5 to 17. Our best fits for these stars are displayed in Figure 3. The fitting technique used here is described at length in BRL97. Briefly, the magnitudes on the CIT system in Table 1 are first transformed onto the Johnson-Glass system using the transformation equations given by Leggett (1992). These magnitudes are then converted into observed fluxes using the method described by Holberg et al. (2006) for photon counting devices but

using the transmission functions taken from Bessell et al. (1990) for the *BVRI* filters on the Johnson-Cousins photometric system, and from Bessell & Brett (1988) for the *JHK* filters on the Johnson-Glass system. The resulting energy distributions are then compared with those predicted from our model atmosphere calculations, properly averaged over the same filter bandpasses. The hydrogen- and helium-rich model atmospheres used in our analysis are similar to those described in BLR01 and references therein, except that for the hydrogen-rich models we are now making use of the more recent H₂-H₂ collision-induced opacity calculations of Borysow et al. (2001) and the Hummer-Mihalas occupation probability formalism for all species in the plasma. We find that the differences in the fitted parameters are small compared to those derived by BLR01, however.

The effective temperature T_{eff} , the solid angle $\pi(R/D)^2$ (with R the radius of the star and D its distance from Earth), and the atmospheric composition (H- or He-rich) are obtained through a χ^2 minimization technique, where the χ^2 value is taken as the sum over all bandpasses of the difference between observed and predicted fluxes, properly weighted by observational uncertainties. The trigonometric parallax measurement, when available, is used to constrain the surface gravity through the mass-radius relation for white dwarfs, otherwise a value of $\log g = 8.0$ is assumed. In Figure 3, the observed *BVRIJK* fluxes are shown as error bars together with the monochromatic model fluxes (for clarity, we do not show the average model fluxes at each bandpass). The derived atmospheric parameters are given in each panel. As can be seen, the energy distributions for all objects can be successfully reproduced by assuming a single star model.

Also reproduced in Figure 3 are the 2MASS magnitudes converted into fluxes using the 2MASS zero points of Holberg et al. (2006). We note that for 9 of the 10 objects, at least one of the fluxes at J , H , or K_S is not compatible with the predicted fluxes *within the 1σ 2MASS uncertainties*. One exception is 0029–032, discussed later in § 3, for which the model spectrum matches the 2MASS photometry even better than the CIT photometry. We thus conclude this section by stating that while the 2MASS photometry is generally reliable, one should expect occasional discrepancies. In particular, the detailed fits (not shown here) to the energy distributions using the 2MASS photometry are of good quality for most stars in our sample.

3. WHITE DWARFS AND LOW MASS MAIN SEQUENCE BINARIES FROM 2MASS

3.1. The Wachter et al. Analysis

One of the most immediate applications to a large data set of white dwarf NIR photometry such as 2MASS is to seek infrared excesses due to cooler companions that are otherwise invisible in the optical. Wachter et al. (2003) used a sample of 759 white dwarfs from the catalog of McCook & Sion (1999) and identified as many as 95 binary candidates and 15 tentative binary candidates based on the analysis of a $(J - H, H - K_S)$ two-color diagram built from 2MASS photometry. They extracted JHK_S magnitudes from the 2MASS second incremental data release. Their binary candidates were selected from the color criterion $(J - H) > 0.4$, defined by the dashed horizontal lines in our Figure 2, while their 15 tentative binary candidates satisfy the criterion $0.2 < (H - K_S) < 0.5$ and $0.1 < (J - H) < 0.4$, defined by the dotted rectangles in Figure 2. In the following, we use the 2MASS final data release to recover more precise and slightly different observed JHK_S magnitudes than those reported by Wachter et al.

Using the same color criteria to study the 2MASS sample of presumably single cool white dwarfs presented in § 2, we find in the upper-right panel of Figure 2 several binary and tentative binary candidates in both regions defined by Wachter et al. (2003). A comparison with the CIT photometry, however, reveals that this result can be readily explained in terms of the larger uncertainties of the 2MASS photometry since both regions are located $1 - 2\sigma$ away from the region occupied by single white dwarfs near the center of the figure. We find that 3.5% and 8.4% of our sample observed by 2MASS contaminate the binary candidate and tentative binary candidate regions, respectively. By comparison, we find that at least 12.5% of the white dwarfs in the complete sample of 759 objects of Wachter et al. are located in the binary candidate region⁴. This indicates that the color criterion defined to identify companions is certainly appropriate, but also that the contamination from faint objects with large uncertainties near the 2MASS detection threshold may be significant. Furthermore, our large contamination of the tentative binary candidate region suggests that this criterion is not stringent enough, and that the corresponding subsample identified by Wachter et al. (2003, Table 2) is mostly composed of single white dwarfs.

These conclusions are supported by the fact that one of the objects selected in the list of binary candidates (0102+210B) and four objects in the list of tentative binary candidates

⁴The actual percentage may be larger depending on how many faint objects with a partial detection are removed from the sample.

(0029–032, 0518+333, 0816+387, and 1247+550)⁵ are all part of the single white dwarf sample described in § 2 and whose fits are displayed in Figure 3. As can be seen, the CIT photometry for all objects is well reproduced with single star model atmospheres. For 0029–032, our fit is even better using the 2MASS photometry than the CIT data. For the other stars, the 2MASS energy distributions appear flatter than those inferred from the CIT photometry or the model spectra, a result that could be interpreted as a flux excess in the K band.

3.2. The Wellhouse et al. Analysis

Using a similar approach but with slightly different criteria, Wellhouse et al. (2005) sought companions to 51 magnetic white dwarfs as candidates for potential pre-cataclysmic variables. They proposed to split the $(J - H, H - K_S)$ two-color diagram into four regions delimiting (I) single white dwarfs, (II) main sequence binary candidates, (III) white dwarfs with very low mass companions, and (IV) objects that may be contaminated by circumstellar material. These representative regions are divided according to previous findings by Wachter et al. (2003) as well as theoretical color simulations. While they did not find any convincing binary candidates (region II), Wellhouse et al. identified six objects with a possible very low mass companion (region III) and four white dwarf candidates with an excess at K_S (region IV), which they interpreted as a signature of undetected planetary nebulae. This represents a total of 28.6% of their sample with formal uncertainties with a possible companion or a disk.

The four regions defined by Wellhouse et al. (2005) are reproduced here in the $(J - H, H - K_S)$ two-color diagram shown in Figure 4, together with our common sample of CIT and 2MASS data composed of presumably single white dwarfs. From this figure, we find that 21% of the white dwarfs in the 2MASS data set would be considered possible candidates for a companion or a disk, while the CIT data show little evidence for such infrared excesses. This strongly suggests that the sample of magnetic white dwarfs studied by Wellhouse et al. could be entirely consistent with single stars. In addition, we note that among the six objects located in region III of Figure 1 from Wellhouse et al. are some of the most intrinsically peculiar white dwarfs⁶: LHS 2229 (1008+290) has been reported by Schmidt et al. (1999)

⁵We also found that the 2MASS identification of 0145–174 by Wachter et al. is erroneous; the actual star is much fainter and not recovered in the 2MASS PSC.

⁶Also, 2201–228 in that sample is probably not magnetic according to S. Jordan (2005, private communication).

and it has the strongest C₂-like features ever observed, LP 790-29 (1036–204) is the strongest magnetic DQ known, and GD 229 (2010+310) shows strong unidentified absorption features in the optical (Wesemael et al. 1993, Fig. 19). Therefore, region III seems to be populated with some of the most peculiar white dwarfs for which there is no reason to expect their NIR colors to overlap with those of normal white dwarfs. Similarly, if we restrict our analysis to the more accurate CIT data, there are three white dwarfs located in region III of our Figure 4. Two of these identified in the figure are also peculiar: G240-72 (1748+708) shows a deep yellow sag in the 4400-6300 Å region (Wesemael et al. 1993, Fig. 19), and LP 701–29 (2251–070) is a heavily blanketed DZ star (Wesemael et al. 1993, Fig. 11).

We also note that all four objects in region IV of Wellhouse et al. (2005, Fig. 1) are very faint stars with 2MASS K_S uncertainties in the range 0.16-0.27. As seen in our Figure 4, we do expect single white dwarfs with large uncertainties to populate this particular region as well. Hence the location of the four objects identified by Wellhouse et al. in this particular region of the ($J - H$, $H - K_S$) two-color diagram is most naturally explained in terms of the low quality of the 2MASS data for these objects rather than the presence of planetary nebulae. We thus conclude that the identification of NIR excesses in the 2MASS PSC database requires more conservative criteria allowing for larger uncertainties in the photometric measurements below the level 1 requirements, or more accurate methods such as that presented in the following section.

3.3. The Synthetic Flux Method

Another technique for identifying binary candidates is to compare observed 2MASS fluxes directly with those predicted from model atmospheres (see. e.g., Holberg et al. 2005, 2006). Effective temperatures and surface gravities are first obtained using the spectroscopic method developed by Bergeron et al. (1992) where high signal-to-noise spectroscopic observations of the hydrogen Balmer lines are fitted with synthetic models. The model flux is then normalized to the observed V magnitude to predict the observed fluxes at J , H , and K_S using the 2MASS filter passbands from Cohen et al. (2003) and the zero points from Holberg et al. (2006). Thus, only objects with known atmospheric parameters and V magnitudes can be used with this method. In what follows, we rely on the fitting technique and NLTE model atmospheres for DA stars described in Liebert et al. (2005) and references therein.

To illustrate the method, we selected all DA stars from Wachter et al. (2003) for which we had an optical spectrum and a published V magnitude. In Table 3, we present our sample that includes 42 binary candidates and 5 tentative binary candidates from Tables

1 and 2 of Wachter et al. (2003), respectively⁷. For each object, we give the atmospheric parameters (T_{eff} and $\log g$), the published V magnitude, and the predicted and observed 2MASS magnitudes at J , H , and K_S . In some cases, the optical spectrum was significantly contaminated by the unresolved companion, and the uncertainties on the derived parameters are correspondingly larger; these are indicated by colons in Table 3.

For most objects, a significant NIR excess is observed, with the 2MASS data being typically ~ 2 magnitudes brighter than the values predicted from the model fits. In Figure 5, we present typical results for ten objects selected from Table 3. Here we show the observed 2MASS fluxes together with the predicted monochromatic fluxes calculated at the atmospheric parameters given in each panel. For 0023+388, 0034–211, 0131–163, and 0145–257, the companion can be unambiguously detected since the 2MASS fluxes are about a factor of 10 to 100 larger than the predicted fluxes. For 0145–221, only a mild NIR excess is observed and this object has indeed been identified as a WD+dL6/7 by Farihi et al. (2005) and Dobbie et al. (2005). Two of the tentative binary candidates, 0710+741 and 2257+162, do indeed show a significant excess consistent with a very low mass companion. Farihi et al. (2005) have actually confirmed that 0710+741 is a WD+dM7. However, for 1434+289, 1639+153, and 2336–187, which are tentative binary candidates in Wachter et al. (2003), we do not observe any significant NIR excess and these objects are thus consistent with being single white dwarfs.

With the exception of these last three objects, the infrared excesses observed in Table 3 are consistent with unresolved low-mass main sequence M dwarfs physically associated with the white dwarfs (Farihi et al. 2006). Photometric observations of single M dwarfs by Leggett et al. (1996) show that the $(J - V)$ color index is in the range from ~ 2 to 4, while single cool white dwarfs are expected to be in the range from -1 to 1. This explains why the contribution of the M dwarf can be dominant in the NIR but negligible in the optical. Many of the 44 remaining binary candidates in Table 3 have been discussed in the literature. For instance, Farihi et al. (2005) and Farihi et al. (2006, with *HST*) observed 28 candidates from this list and were able to resolve the red dwarf companion(s) for 17 objects. The NIR excesses were also confirmed by Farihi et al. (2005, 2006) using *JHK* photometric observations for the 11 remaining unresolved objects. The presence of a companion for 9 additional objects in Table 3 has been discussed at various degrees in the literature, while for the 7 remaining binary candidates (0812+478, 0915+201, 1037+512, 1108+325, 1339+346, 1610+383, and

⁷Note that the 2MASS identification for 40 Eri B (0413+077) by Wachter et al. is erroneous. With two objects within $2''$, they picked what is probably the M dwarf 40 Eri C instead of 40 Eri B itself. Thus, while this is still technically a WD+dM binary, both objects are barely resolved in 2MASS and we do not include them in our sample.

2257+162), we confirm through the synthetic flux method a strong NIR excess consistent with the presence of low mass main-sequence companions.

We have seen that for a brown dwarf companion, the flux excess is not as important as for M dwarfs. In the case of the dL6/7 dwarf companion to 0145–221, the flux excess at K_S is still significant at the 12σ level, however, according to Table 3. There is only one known example of a companion with a possible later spectral type, the brown dwarf companion to 0137–349, discovered from radial velocity measurements by Maxted et al. (2006), who also report a small excess at K_S from 2MASS PSC data. Burleigh et al. (2006) also present a near-IR spectrum that confirms the slight K -band excess they attribute to a dL8 companion. We analyzed the 2MASS photometry of this object with the method described in this section, and assumed the effective temperature and surface gravity from Maxted et al. (2006). We were able to match very well the predicted and observed 2MASS J magnitude within the uncertainties, and also identified a flux excess at K_S at the 2.49σ level, which is barely significant, but still consistent with the presence of a disk or a companion. Therefore, the 2MASS survey is able to identify hot brown dwarf companions, but it becomes more difficult to confirm their presence for spectral types later than about dL7.

We end this section by asserting that methods based on comparisons of observed and predicted 2MASS fluxes (or magnitudes) represent an efficient way of identifying unresolved white dwarf and low-mass main sequence binaries down to late-type L dwarfs. Our analysis also reveals, however, that $(J-H, H-K_S)$ two-color diagrams based on 2MASS data should be interpreted with caution, and that regions expected to contain unresolved binaries may be contaminated with single white dwarfs, especially when data below the level 1 requirements are considered.

4. INFRARED PHOTOMETRY FROM SPITZER

The *Spitzer Space Telescope* has been used to secure for the first time IRAC 4.5 and 8 μm photometric data for relatively bright, nearby white dwarfs (see, e.g., Hansen et al. 2006). One of the main interests of these surveys is to look for infrared flux excesses due to the presence of circumstellar disks since it is expected that the cool disk would dominate the MIR flux. It is however necessary as a first step to evaluate the reliability of the *Spitzer* data set and the ability of the model atmospheres to reproduce the MIR fluxes. In such an effort, Kilic et al. (2006b) compared the *Spitzer* 4.5 and 8 μm photometric data of 18 cool and bright white dwarfs with the predictions of model atmospheres. They found that the four hydrogen atmosphere white dwarfs with $T_{\text{eff}} \lesssim 6000$ K show a slight flux depression at 8 μm , while one peculiar object, the so-called C₂H star LHS 1126, suffers from a significant flux

deficit at both 4.5 and 8 μm . For the warmer objects, the model fluxes seem to reproduce the *Spitzer* data perfectly.

In this section, we reanalyze 14 objects from the sample of Kilic et al. (2006b) for which optical *BVRI* photometry and infrared *JHK* photometry on the CIT system are available (all of these are already part of our cool white dwarf sample discussed in § 2). In an approach similar to that described in § 2 (see Fig. 3), we determine the atmospheric parameters for each star by fitting simultaneously the average fluxes for the nine photometric bands (*BVRI*, *JHK*/CIT, and *Spitzer* 4.5 and 8 μm). The synthetic fluxes in the MIR are obtained by integrating our model grid over the *Spitzer* IRAC spectral response curves while the observed fluxes are taken directly from Table 1 of Kilic et al. (2006b). In contrast with the technique used by Kilic et al., we do not normalize the fluxes at any particular band, but consider instead the solid angle $\pi(R/D)^2$ a free parameter. Since our χ^2 value is taken as the sum over all bands of the difference between observed and model fluxes, properly weighted by the corresponding observational errors, our approach has the advantage of allowing for the full photometric uncertainties in the fitting procedure. Furthermore, instead of assuming $\log g = 8.0$ for all objects, we constrain the $\log g$ value from the trigonometric parallax measurements, as described above.

In Figure 6, we present our best fits on a logarithmic scale to the observed *BVRI*, *JHK* (CIT), and *Spitzer* photometry with the model average fluxes described above. We also plot the monochromatic fluxes for clarity; the case of LHS 1126 is discussed separately below. Another peculiar object, G240-72 (1748+708) already discussed near the end of § 3.2, shows a deep unidentified absorption in the optical (a yellow sag) and no satisfactory fit can be achieved for this star and it is thus left out of our analysis. For Ross 627 (1121+216), the 8 μm flux is not shown in Figure 6 since Kilic et al. (2006b) provides only an upper limit due to a possible contamination from a nearby star. Our final sample thus includes 12 stars with 23 *Spitzer* 4.5 and 8 μm flux measurements. For all cases shown in Figure 6, the *Spitzer* fluxes are well reproduced by the synthetic models. To further strengthen this conclusion, we plot in Figure 7 the ratio of the observed to model fluxes at 4.5 and 8 μm as a function of the derived effective temperature for the 12 objects. The figure confirms the agreement between the observed *Spitzer* and model fluxes at all temperatures. In particular, we do not observe any significant flux deficit at low effective temperatures as suggested by Kilic et al. (2006b). There are only 2 observations out of 23 for which the flux deficit is significant at the 1σ level, and both are in the 8 μm band. It thus seems premature to conclude from these results that there is any discrepancy between the observations and the predictions of model atmospheres with pure hydrogen compositions.

We mention in this context that the second coolest object in Figure 7 is the DA star BPM

4729 (0752–676) for which we obtain a perfect fit. This star has been studied extensively by BLR01, and more recently by Kowalski & Saumon (2006) using improved $L\alpha$ profiles that include broadening by molecular hydrogen, and both atmospheric parameter determinations agree at the 1σ level under the assumption of pure hydrogen compositions. Hence for this well studied normal cool DA star, independent model atmospheres yield consistent atmospheric parameters that both match the observational data. In contrast, the two objects — LHS 1038 (0009+501) and G99-47 (0553+053) — with the small $8\ \mu\text{m}$ flux discrepancies (bottom panel of Fig. 7) are magnetic white dwarfs. Both objects show 1σ discrepancies at J and also at B for G99-47. While this suggests that the inclusion of a magnetic field in the model atmosphere calculations could improve the fit, we believe that the discrepancies observed here are only barely significant and not systematic enough to make formal conclusions. Therefore, we argue that the results presented in this section demonstrate the reliability of both the *Spitzer* IRAC photometry and our model atmosphere grid up to $8\ \mu\text{m}$ for studying cool white dwarfs. The consistency between models and data is critical for surveys seeking MIR infrared excesses from circumstellar disks. Our results indicate that the comparison of *Spitzer* fluxes with theoretical predictions could identify such MIR excesses with relatively high precision.

In an attempt to identify the nature of the discrepancy between our conclusions and those reached by Kilic et al. (2006b), we have performed the same analysis as above but with the 2MASS JHK_s magnitudes used by Kilic et al. (instead of the CIT magnitudes used in this analysis). We have also tried to normalize our solutions at V , as done by Kilic et al. In all of our experiments, the results differ only slightly from those reported here, and our main conclusions thus remain the same. We are therefore unable to explain the differences between both studies. We can only emphasize that the analysis of *Spitzer* photometric data appears to be sensitive to the details of the fitting procedure.

Another white dwarf analyzed by Kilic et al. (2006b) is LHS 1126 (0038–226) whose energy distribution is characterized by a strong infrared flux deficiency at JHK interpreted by Bergeron et al. (1994) in terms of collision-induced absorption (CIA) by molecular hydrogen due to collisions with helium in a mixed hydrogen and helium atmosphere with $N(\text{H})/N(\text{He}) \sim 0.01$. We do confirm here the results shown in Figure 4 of Kilic et al. (2006b) where the *Spitzer* fluxes are significantly depressed with respect to the predictions of model atmospheres with mixed compositions. The main reason for this discrepancy is that the CIA opacity predicts a *maximum* absorption near the H_2 fundamental vibration frequency at $\sim 2.4\ \mu\text{m}$, while the *Spitzer* fluxes are more consistent with a featureless energy distribution from 1 to $8\ \mu\text{m}$. This problem is surprisingly similar to that encountered in the so-called ultra-cool white dwarfs, and in particular in the case of LHS 3250 for which the $\text{H}_2\text{-H}_2$ and $\text{H}_2\text{-He}$ CIA opacities predict absorption bands that are simply not observed in

spectroscopy (Bergeron et al. 2002). These results may indicate that the collision-induced opacity calculations need to be improved at the high densities encountered in cool white dwarf atmospheres.

5. CANDIDATE WHITE DWARFS WITH CIRCUMSTELLAR DISKS

The synthetic flux method based on a comparison of predicted and observed 2MASS fluxes (or magnitudes) was shown to be an efficient technique for detecting NIR excesses from unresolved companions (§ 3). However, the NIR excess in the JHK_S bands expected from cool circumstellar disks or planets surrounding white dwarf stars can be extremely small if the flux is dominated by the white dwarf in this particular wavelength range. In this section, we use the results of the ongoing spectroscopic survey of Gianninas et al. (2006) together with the 2MASS PSC to search for massive disks resulting from the merger of two white dwarfs, as predicted by Livio et al. (2005). In addition to the synthetic flux method described above, we also compare the observed and predicted $(J - H)$ and $(J - K_S)$ color indices since this method has the advantage of being independent of the normalization at V , which allows us to consider also objects with no published V magnitudes. Since circumstellar disks are expected to be much brighter at K_S than in the other bands, we expect their color indices to be very different from those of single white dwarfs, and such objects should easily stand out in our analysis.

As discussed in the Introduction, white dwarfs resulting from mergers are expected to be found in the high-mass tail of the mass distribution. We thus selected all DA stars from the survey of Gianninas et al. (2006) with spectroscopic masses above $0.8 M_\odot$ that were formally detected by 2MASS in at least two bands (usually the J and H bands), for a total of 57 objects. In Table 4, we provide the effective temperature, the spectroscopic mass, the V magnitude (when available), as well as the predicted and observed 2MASS JHK_S magnitudes for each object in our sample. The atmospheric parameters (T_{eff} and $\log g$) are obtained from fits to the Balmer lines using the NLTE model grid described in § 3, and the $\log g$ values are converted into mass using the evolutionary models of Wood (1995) with carbon-core compositions and thick hydrogen layers. The predicted fluxes are obtained from the synthetic flux method and are thus only given for objects with measured V magnitudes.

Five white dwarfs in Table 4 (0429+176, 0950+139, 1058–129, 1120+439, and 1711+668) show a large NIR flux excess that is not attributable to a circumstellar disk. The predicted spectra for these stars are shown in Figure 8 together with the observed 2MASS fluxes. We discuss each object in turn.

HZ 9 (0429+176) – This object is a WD+dM binary (Lanning et al. 1981) in common with the sample discussed in § 3.

PG 0950+139 – This star is in common with the sample discussed in § 3. The white dwarf is surrounded by a planetary nebulae (Ellis et al. 1984) and its optical spectrum exhibits emission lines (Liebert et al. 1989). According to Fulbright et al. (1993), the low-density gas emission and the infrared excess are best explained by the presence of a low-mass companion.

PG 1058–129, *PG 1120+439* – These two objects show a mild and unexplained infrared excess. In both cases, the only V magnitudes available are multichannel data from the Palomar-Green survey (Green et al. 1986). Since the observed energy slopes measured by color indices are in perfect agreement with those predicted by the models (see below), it is very likely that the V magnitudes for these stars are simply erroneous. We note that Green et al. (2000) also determined a 1-sigma significant excess at J for PG 1120+439.

RE J1711+664 (1711+668) – This white dwarf is a barely resolved visual pair (Finley et al. 1997). The predicted NIR flux from this white dwarf is too low to be detected by 2MASS. Thus only the dM star $\sim 2''$ away from the white dwarf is detected in the PSC.

We exclude from our analysis the three objects with known companions, but we keep PG 1058–129 and PG 1120+439.

We compare in Figure 9 the observed and predicted ($J-H$) and ($H-K_S$) color indices as a function of H and K_S , respectively, for the remaining 54 white dwarfs in our sample. An examination of these results indicate that all stars are consistent with the predicted white dwarf colors within 3σ uncertainties, both above and below the level 1 requirements. Two glaring exceptions are G1-7 (0033+016) and CBS 413 (1554+322), which are among the faintest objects in the bottom panel of Figure 9 (labeled 1 and 2, respectively). For G1-7, however, the color indices derived from the CIT photometry given in Table 1 are in excellent agreement with those predicted by the models. Also, CBS 413 has not been detected at H but it is unexpectedly bright at K_S ! Since this object has no published V magnitude, it is not clear whether the J detection is indeed from the white dwarf, and thus whether the color excess at K_S is even real. Therefore, we conclude from the results shown in Figure 9 that there is no strong evidence for H or K_S excesses in this sample of massive white dwarfs, and for the presence of massive circumstellar disks around them.

For comparison, we also reproduce in Figure 9 the location of three white dwarfs with previously identified circumstellar disks: G29-38 (2326+049), GD 362 (1729+371) and GD 56 (0408–041). The atmospheric parameters for all three stars have been determined using our own spectroscopic observations, and the predicted 2MASS color indices have been estimated from the same method as above. For the metal-rich DAZ star GD 362, we use

the more accurate atmospheric parameters of Gianninas et al. (2004) who took into account the presence of heavy elements in their model atmosphere calculations. Only GD 362 in our sample is a massive white dwarf with $M = 1.24 M_{\odot}$, while we obtain $M = 0.70$ and $0.60 M_{\odot}$ for G29-38 and GD 56, respectively. The disk around G29-38 was the first discovered and studied extensively in the MIR (Reach et al. 2005). The object is clearly identifiable in Figure 9 with $(J - K_S)_{2\text{MASS}} - (J - K_S)_{\text{pred}} = 0.52 \pm 0.04$, a $\sim 12\sigma$ result. The second object, GD 362, is a massive DAZ star for which Becklin et al. (2005) reported the discovery of an important flux excess at L' ($3.76 \mu\text{m}$) and N' ($11.3 \mu\text{m}$). Kilic et al. (2005) obtained a near infrared spectrum in the $0.8 - 2.5 \mu\text{m}$ range but found only a mild flux excess at K . Both studies concluded that the presence of a dust disk could account for the observations. Given that GD 362 is particularly faint ($V = 16.3$), only lower limits at H and K_S are available in the 2MASS PSC. Instead, we use in Figure 9 the JHK_S magnitudes measured by Becklin et al. (2005). With these measurements, GD 362 exhibits a color excess of $(J - K_S)_{\text{obs}} - (J - K_S)_{\text{pred}} = 0.22 \pm 0.04$, a 5σ result. Unfortunately, this photometric accuracy is only achieved in the 2MASS sample for J brighter than ~ 14.1 , and a color excess of the magnitude found in GD 362 cannot be easily uncovered in the majority of white dwarfs detected by 2MASS. For GD 56, Kilic et al. (2006a) reported a NIR excess in both the 2MASS data and in their own infrared spectroscopic observations. Unlike the two previous objects, GD 56 lacks the MIR observations that could confirm the presence of a disk. We recovered the 2MASS magnitudes from the PSC and determined a color excess of $(J - K_S)_{2\text{MASS}} - (J - K_S)_{\text{pred}} = 0.54 \pm 0.19$, a 2.9σ result, barely significant according to our 3σ criterion.

From the analysis of the three known white dwarfs with circumstellar disks, we conclude that the infrared excess from similar disks around white dwarfs would be significant only for bright level 1 2MASS objects. We argue that while the 2MASS PSC is indeed able to suggest the presence of a disk for fainter stars like GD 56, MIR photometric observations or more accurate NIR data would be required to unambiguously identify circumstellar disks such as those discussed here. Furthermore, according to Livio et al. (2005), a circumstellar disk resulting from the merger of two white dwarfs would presumably have a much larger mass and radius in comparison with the disks currently known. Hence the expected NIR excess should also be large. Obviously, such large infrared excesses have not been detected in our 2MASS sample, and we conclude that massive circumstellar disks are uncommon around massive white dwarfs, in agreement with the conclusions reached by Hansen et al. (2006) based on *Spitzer* data. While our results constrain the scenario proposed by Livio et al. (2005), the fraction of massive degenerates in our sample that are the product of white dwarf mergers is totally unknown. For instance, Dobbie et al. (2006) suggested that GD 50 (0346–011) is associated with the star formation event that created the Pleiades, and this

massive white dwarf is most likely a former member of this cluster. Hence the authors find no need to invoke a double white dwarf merger scenario to account for its existence. Thus, massive circumstellar disks may not be expected in all cases studied here.

6. CONCLUSION

In order to estimate the reliability of the 2MASS photometry for white dwarf stars, we defined a sample of 160 cool degenerates with JHK magnitudes on the CIT photometric system taken from BRL97 and BLR01, and compared these values with those obtained from the 2MASS PSC. Our statistical analysis indicates that, on average, both data sets are consistent within the uncertainties, and thus that the 2MASS photometric data is appropriate for the study of white dwarf stars. The 2MASS data should still be interpreted with caution, however, especially for stars near the detection threshold, as significant discrepancies are to be expected.

We also concluded that the search for white dwarf and main-sequence star binaries based on 2MASS two-color diagrams is greatly limited by the 2MASS uncertainties when data below the level 1 requirements are considered. We demonstrated that some color regions identified by Wachter et al. (2003) and Wellhouse et al. (2005) to search for binary candidates are highly contaminated by single stars. We analyzed 47 binary candidates taken from the sample of Wachter et al. (2003) using the synthetic flux method and showed that this technique is a much more efficient tool for confirming binary candidates. We have also shown that the observed MIR photometry from the *Spitzer Space Telescope* agree very well with our model fluxes, a result that confirms the reliability of both the *Spitzer* photometry and our model atmosphere calculations up to $8 \mu\text{m}$.

Finally, we searched for massive and large circumstellar disks, such as those predicted by Livio et al. (2005), around 57 massive white dwarfs ($M > 0.8 M_{\odot}$). We showed that these systems would be clearly distinguishable from single stars in the 2MASS PSC, but such systems have not yet been identified in our analysis. Hence, high-mass circumstellar disks resulting from the merger of two white dwarfs must be uncommon around massive white dwarfs. We also showed that low-mass circumstellar disks such as those associated with G29-38, GD 362 and GD 56 are only barely identifiable except perhaps for the brightest level 1 white dwarfs in the 2MASS PSC.

We would like to thank A. Gianninas for a careful reading of our manuscript and for sharing the results of his ongoing spectroscopic survey. This work was supported in part by the NSERC Canada. P. Bergeron is a Cottrell Scholar of Research Corporation. This

publication makes use of data products from the Two Micron All Sky Survey, which is a joint project of the University of Massachusetts and the Infrared Processing and Analysis Center/California Institute of Technology, funded by the National Aeronautics and Space Administration and the National Science Foundation. This work is based in part on observations made with the *Spitzer Space Telescope*, which is operated by the Jet Propulsion Laboratory, California Institute of Technology under a contract with NASA.

REFERENCES

- Becklin, E. E., Farihi, J., Jura, M., Song, I., Weinberger, A. J., & Zuckerman, B. 2005, *ApJ*, 632, L119
- Bergeron, P., & Leggett S. K. 2002, *ApJ*, 580, 1070
- Bergeron, P., Leggett S. K., & Ruiz, M. T. 2001, *ApJS*, 133, 413 (BLR01)
- Bergeron, P., Ruiz, M. T., & Leggett S. K. 1997, *ApJS*, 108, 339 (BRL97)
- Bergeron, P., Ruiz, M. T., Leggett, S. K., Saumon, D., & Wesemael, F. 1994, *ApJ*, 423, 456
- Bergeron, P., Saffer, R. A., & Liebert, J. 1992, *ApJ*, 394, 228
- Bessell, M. S. 1990, *PASP*, 102, 1181
- Bessell, M. S., & Brett, J. M. 1988, *PASP*, 100, 1134
- Borysow, A., Jorgensen, U. G., & Fu, Y. 2001, *JQSRT*, 68, 235
- Burleigh, M. R., Hogan, E., Dobbie, P. D., Napiwotzki, R., & Maxted, P. F. L. 2006, *MNRAS*, 373, L55
- Carpenter J. M. 2001, *AJ*, 121, 2851
- Chary, R., Zuckerman, B., & Becklin, E. E. 1999, in *The Universe as Seen by ISO*, ed. P. Cox & M. F. Kessler (ESA SP-427; Noordwijk: ESA/ESTEC), p. 289
- Cohen, M., Wheaton, W. A., Megeath, S. T. 2003, *AJ*, 126, 1090
- de La Fuente Marcos, R., & de La Fuente Marcos, C. 2005, *New Astronomy*, 11, 59
- Debes, J. H., Sigurdsson, S., & Woodgate, B. E. 2005, *AJ*, 130, 1221

- Dobbie, P. D., Burleigh, M. R., Levan, A. J., Barstow, M. A., Napiwotzki, R., Holberg, J. B., Hubeny, I., & Howell, S. B. 2005, *MNRAS*, 357, 1049
- Dobbie, P. D., Napiwotzki, R., Lodieu, N., Burleigh, M. R., Barstow, M. A. & Jameson, R. F. 2006, *MNRAS*, 373, L45
- Ellis, G. L., Grayson, E. T., & Bond, H. E. 1984, *PASP*, 96, 283
- Farihi, J., Becklin, E. E., & Zuckerman, B. 2005, *ApJS*, 161, 394
- Farihi, J., Hoard, D. W., & Wachter, S. 2006, *ApJ*, 646, 480
- Finley, D. S., Koester, D., & Basri, G. 1997, *ApJ*, 488, 375
- Fulbright, M. S., & Liebert, J. 1993, *ApJ*, 410, 275
- Gianninas, A., Bergeron, P., & Fontaine, G. 2006, *AJ*, 132, 831
- Gianninas, A., Dufour, P., & Bergeron, P. 2004, *ApJ*, 617, L57
- Green, P. J., Ali, B., & Napiwotzki R. 2000, *ApJ*, 540, 992
- Green, R. F., Schmidt, M., & Liebert, J. 1986, *ApJS*, 61, 305
- Hansen, B. M. S., Kulkarni, S., & Wiktorowicz S. 2006, *AJ*, 131, 1106
- Holberg, J. B., & Bergeron, P. 2006, *AJ*, 132, 1223
- Holberg, J. B., & Margargal, K. 2005, 14th European Workshop on White Dwarfs, ASP Conference Series, Vol. 334, eds. D. Koester & S. Moehler (San Francisco: Astronomical Society of the Pacific), 419
- Jura, M. 2003, *ApJ*, 584, L91
- Kilic, M., von Hippel, T., Leggett, S. K., & Winget, D. E. 2005, *ApJ*, 632, L115
- Kilic, M., von Hippel, T., Leggett, S. K., & Winget, D. E. 2006a, *ApJ*, 646, 47
- Kilic, M., von Hippel, T., Mullally, F., Reach, W. T., Kuchner, M. J., Winget, D. E., & Burrows, A. 2006b, *ApJ*, 642, 1051
- Kowalski, P., & Saumon, D. 2006, *ApJ*, 651, L137
- Lanning H. H., & Pesch P. 1981, *ApJ*, 244, 280
- Leggett, S. K. 1992, *ApJS*, 82, 351

- Leggett, S. K., Allard, F., Berriman, G., Dahn, C. C., & Hauschildt, P. H. 1998, *ApJS*, 104, 117
- Leggett S. K., Ruiz, M. T., & Bergeron, P. 1998, *ApJ*, 497, 294
- Liebert, J., Bergeron, P., & Holberg, J. B. 2005, *ApJS*, 156, 47
- Liebert, J., Green, R., Bond, H. E., Holberg, J. B., Wesemael, F., Fleming, T. A., & Kidder, K. 1989, *ApJ*, 346, 251
- Livio, M., Pringle, J. E., & Wood, K. 2005, *ApJ*, 632, L37
- Maxted, P. F. L., Napiwotzki, R., Dobbie, P. D., & Burleigh, M. R. 2006, *Nature*, 442, 543
- McCook G. P., & Sion E. M. 1999, *ApJS*, 121, 1
- Reach, W. T., Kuchner, M. J., von Hippel, T., Burrows, A., Mullally, F., Kilic, M., & Winget, D. E. 2005, *ApJ*, 635, L161
- Schmidt, G. D., Liebert, J., Harris, H. C., Dahn, C. C., Leggett, S. K. 1999, *ApJ*, 512, 916
- Silvestri, N. M., Oswalt, T. D., & Hawley, S. L. 2002, *AJ*, 124, 1118
- Wachter, S., Hoard, D. W., Hansen, K. H., Wilcox, R. E., Taylor, H. M., & Finkelstein, S. L. 2003, *ApJ*, 586, 1356
- Wellhouse, J. W., Hoard, D. W., Howell, S., B., Wachter, S., & Esin, A. A. 2005, *PASP*, 117, 1378
- Wesemael, F., Greenstein, J. L., Liebert, J., Lamontagne, R., Fontaine, G., Bergeron, P., & Glaspey, J. W. 1993, *PASP*, 105, 761
- Wickramasinghe, D. T. & Ferrario, L. 2000, *PASP*, 112, 873
- Wood, M. A. 1995, in *Proceedings of the 9th European Workshop on White Dwarfs*, eds. D. Koester & K. Werner (Berlin: Springer), 41
- Zuckerman, B., & Becklin, E. E. 1992, *ApJ*, 386, 260
- Zuckerman, B., & Becklin, E. E. 1987, *Nature*, 330, 138

Table 1. Sample of Cool White Dwarfs with Near-Infrared Photometry

WD	Name	J_{CIT}	H_{CIT}	K_{CIT}	$J_{2\text{MASS}} (\sigma_J)$	$H_{2\text{MASS}} (\sigma_H)$	$K_{S2\text{MASS}} (\sigma_K)$
0000–345	LHS 1008	14.17	14.02	13.87	14.117 (0.024)	14.024 (0.038)	13.919 (0.063)
0007+308	LHS 1028	16.43	16.34	16.33	16.449 (0.128)	16.193 (0.224)	16.614 (null)
0009+501	LHS 1038	13.41	13.26	13.21	13.490 (0.022)	13.249 (0.026)	13.191 (0.030)
0011+000	G31-35	15.21	15.13	15.12	15.148 (0.039)	15.214 (0.094)	15.101 (0.139)
0011–134	LHS 1044	14.85	14.62	14.52	14.813 (0.036)	14.549 (0.057)	14.628 (0.082)
0029–032	LHS 1093	15.56	15.37	15.35	15.635 (0.050)	15.380 (0.091)	15.166 (0.147)
0033+016	G1-7	15.63	15.60	15.63	15.650 (0.057)	15.522 (0.090)	16.119 (0.303)
0038–226	LHS 1126	13.32	13.47	13.71	13.342 (0.028)	13.483 (0.033)	13.738 (0.044)
0038+555	G218-8	13.97:	14.08:	14.13:	14.066 (0.036)	13.981 (null)	13.967 (null)
0046+051	vMa 2	11.69	11.61	11.52	11.688 (0.022)	11.572 (0.024)	11.498 (0.025)
0048–207	LHS 1158	15.76	15.38	15.38	15.748 (0.060)	15.378 (0.090)	15.216 (0.125)
0101+048	G1-45	13.51	13.39	13.38	13.504 (0.024)	13.396 (0.032)	13.418 (0.034)
0102+210A	LHS 5023	16.56:	16.32:	16.21:	16.518 (0.097)	16.504 (0.198)	15.548 (null)
0102+210B	LHS 5024	16.45:	16.12:	16.00:	16.734 (0.110)	16.267 (0.164)	15.589 (0.188)
0112–018	LHS 1219	16.29	16.00	15.97	16.288 (0.089)	15.763 (0.136)	15.974 (0.261)
0115+159	LHS 1227	13.72	13.72	13.74	13.727 (0.025)	13.680 (0.022)	13.726 (0.044)
0117–145	LHS 1233	15.47	15.17	15.08	15.563 (0.056)	15.131 (0.079)	15.192 (0.161)
0121+401	G133-8	15.64	15.43	15.41	15.858 (0.078)	15.507 (0.151)	15.279 (0.170)
0123–262	LHS 1247	14.50	14.36	14.38	14.435 (0.029)	14.313 (0.044)	14.331 (0.072)
0126+101	G2-40	14.05	13.92	13.94	14.032 (0.024)	13.952 (0.038)	13.964 (0.053)
0135–052	L870-2	12.12	11.94	11.92	12.114 (0.024)	11.954 (0.022)	11.969 (0.023)
0142+312	G72-31	14.38	14.33	14.38	14.425 (0.029)	14.320 (0.048)	14.429 (0.065)
0208+396	G74-7	13.80	13.65	13.63	13.832 (0.024)	13.670 (0.034)	13.595 (0.038)
0222+648	LHS 1405	16.35	16.06	15.98	16.357 (0.100)	15.572 (0.125)	15.729 (0.212)
0230–144	LHS 1415	14.43	14.17	14.11	14.489 (0.030)	14.261 (0.048)	14.161 (0.068)
0243–026	LHS 1442	14.71	14.49	14.51	14.679 (0.035)	14.589 (0.044)	14.477 (0.091)
0245+541	LHS 1446	13.89	13.66	13.60	13.870 (0.024)	13.545 (0.040)	13.469 (0.039)
0322–019	G77-50	14.63	14.37	14.28	14.761 (0.042)	14.439 (0.052)	14.378 (0.084)
0326–273	L587-77A	13.27	13.12	13.08	13.216 (0.103)	13.109 (0.090)	13.101 (0.121)
0341+182	Wolf 219	14.56	14.35	14.40	14.590 (0.031)	14.350 (0.049)	14.230 (0.060)
0357+081	LHS 1617	14.59	14.33	14.26	14.562 (0.038)	14.343 (0.056)	14.122 (0.057)
0407+197	LHS 1636	16.26	16.03	15.82	16.130 (0.084)	15.957 (0.161)	15.178 (null)
0423+044	LHS 1670	15.50	15.29	15.26	15.474 (0.068)	15.182 (0.075)	15.168 (0.150)
0423+120	G83-10	14.52	14.34	14.27	14.485 (0.034)	14.347 (0.042)	14.249 (0.065)
0433+270	G39-27	14.61	14.32	14.22	14.598 (0.038)	14.232 (0.058)	14.136 (0.069)
0435–088	L879-14	13.00	12.85	12.79	13.006 (0.030)	12.906 (0.032)	12.763 (0.035)
0437+093	LHS 1693	16.03	15.80	15.81	15.944 (0.075)	15.583 (0.102)	15.583 (0.158)
0440+510	G175-46	15.60	15.50	15.53	15.576 (0.051)	15.504 (0.112)	15.548 (0.141)
0503–174	LHS 1734	14.55	14.33	14.23	14.739 (0.035)	14.408 (0.047)	14.397 (0.086)
0511+079	G84-41	15.01	14.79	14.71	15.107 (0.047)	14.924 (0.064)	14.863 (0.082)
0518+333	G86-B1B	15.52	15.33	15.34	15.374 (0.085)	15.122 (0.207)	14.806 (0.157)
0548–001	G99-37	13.73	13.63	13.63	13.730 (0.029)	13.675 (0.026)	13.705 (0.043)
0551+468	LHS 1801	15.84	15.55	15.53	15.712 (0.057)	15.461 (0.078)	15.511 (0.154)
0552–041	LP 658-2	13.02	12.90	12.82	13.047 (0.027)	12.860 (0.027)	12.777 (0.026)
0553+053	G99-47	12.96	12.77	12.66	12.930 (0.022)	12.720 (0.025)	12.653 (0.024)
0618+067	LHS 1838	15.29	15.05	15.00	15.377 (0.062)	15.017 (0.071)	14.957 (0.139)

Table 1—Continued

WD	Name	J_{CIT}	H_{CIT}	K_{CIT}	$J_{2\text{MASS}} (\sigma_J)$	$H_{2\text{MASS}} (\sigma_H)$	$K_{S2\text{MASS}} (\sigma_K)$
0644+025	G108-26	15.00	14.85	14.93	14.868 (0.045)	14.757 (0.069)	14.576 (0.103)
0648+641	LP 58-53	15.46	15.19	15.12	15.533 (0.061)	15.412 (0.098)	15.331 (0.165)
0654+027	G108-42	15.98	15.98	15.98	16.086 (0.088)	15.824 (0.133)	15.399 (0.188)
0657+320	LHS 1889	14.99	14.77	14.69	15.030 (0.039)	14.674 (0.050)	14.665 (0.082)
0659-064	LHS 1892	14.58	14.29	14.24	14.538 (0.028)	14.218 (0.051)	14.355 (0.074)
0704-508	ESO 207-124	16.24::	16.11::	null	16.08 (0.062)	16.093 (0.131)	15.688 (0.196)
0706+377	G87-29	15.00	14.88	14.82	15.064 (0.053)	14.783 (0.052)	14.834 (0.079)
0738-172	L745-46A	12.65	12.61	12.52	12.653 (0.022)	12.611 (0.026)	12.583 (0.036)
0747+073A	LHS 240	14.96	14.73	14.72	14.996 (0.039)	14.719 (0.067)	14.634 (0.099)
0747+073B	LHS 239	15.05	14.90	14.86	15.031 (0.037)	14.898 (0.080)	14.746 (0.107)
0751+578	G193-78	14.94	14.94	14.96	14.966 (0.038)	14.965 (0.063)	14.966 (0.121)
0752-676	BPM 4729	12.79	12.52	12.43	12.726 (0.023)	12.476 (0.026)	12.362 (0.024)
0752+365	G90-28	15.50	15.35	15.35	15.583 (0.064)	15.444 (0.131)	15.877 (0.346)
0802+386	LP 257-28	15.60	15.58	15.64	15.376 (null)	15.663 (0.150)	15.046 (null)
0802+387	LHS 1980	15.26	15.02	14.96	15.336 (0.047)	15.193 (0.079)	14.899 (0.091)
0806-661	L97-3	13.79	13.85	13.92	13.704 (0.023)	13.739 (0.025)	13.781 (0.043)
0813+217	G40-15	16.03	15.74	15.65	15.944 (0.068)	15.842 (0.142)	15.958 (0.240)
0816+387	G111-71	15.87	15.72	15.73	16.070 (0.103)	15.833 (0.194)	15.583 (0.220)
0827+328	LHS 2022	15.01	14.85	14.84	14.985 (0.044)	14.964 (0.076)	14.865 (0.121)
0839-327	L532-81	11.59	11.55	11.55	11.578 (0.030)	11.539 (0.033)	11.547 (0.029)
0856+331	G47-18	15.12	15.09	15.11	15.172 (0.041)	15.156 (0.083)	15.312 (0.163)
0912+536	G195-19	13.22	13.15	13.09	13.308 (0.025)	13.211 (0.026)	13.133 (0.030)
0913+442	G116-16	14.96	14.84	14.87	14.955 (0.050)	14.861 (0.081)	14.906 (0.155)
0930+294	G117-25	15.51	15.40	15.45	15.588 (0.066)	15.399 (0.106)	15.284 (0.150)
0941-068	G161-68	15.35	15.06	15.08	15.373 (0.042)	15.019 (0.069)	14.990 (0.133)
0946+534	G195-42	14.90	14.87	14.88	14.913 (0.049)	14.888 (0.072)	14.916 (0.118)
0955+247	G49-33	14.66	14.59	14.65	14.654 (0.034)	14.659 (0.069)	14.661 (0.076)
1012+083	G43-38	15.20	14.99	14.94	15.246 (0.063)	15.132 (0.110)	14.955 (0.142)
1019+637	LP 62-147	13.83	13.63	13.65	13.874 (0.029)	13.733 (0.047)	13.692 (0.049)
1026+117	LHS 2273	15.93	15.83	15.68	15.902 (0.095)	15.552 (0.127)	15.298 (null)
1039+145	G44-32	15.93	15.86	15.78	15.823 (0.069)	15.749 (0.156)	15.681 (0.205)
1055-072	LHS 2333	13.81	13.71	13.69	13.770 (0.029)	13.680 (0.032)	13.485 (0.038)
1108+207	LHS 2364	15.91	15.69	15.62	15.978 (0.074)	15.532 (0.107)	15.565 (0.161)
1114+067	G45-45	15.82	15.57	15.54	15.701 (0.072)	15.599 (0.124)	15.518 (0.257)
1115-029	LHS 2392	15.23	15.27:	15.29:	15.304 (0.051)	15.246 (0.084)	15.734 (0.241)
1121+216	Ross 627	13.58	13.40	13.40	13.574 (0.024)	13.420 (0.026)	13.399 (0.034)
1124-296	ESO 439-80	14.90	14.88	14.80	14.782 (0.034)	14.710 (0.044)	14.602 (0.091)
1142-645	LHS 43	11.19	11.12	11.09	11.188 (0.024)	11.130 (0.025)	11.104 (0.026)
1146-291	ESO 440-146	16.17	15.89:	15.71:	16.037 (0.092)	15.737 (0.172)	16.462 (null)
1147+255	LP 375-51	15.53	15.49	15.51	15.590 (0.048)	15.568 (0.101)	15.693 (0.183)
1153+135	LHS 2478	16.10	15.83	15.74:	15.889 (0.062)	15.503 (0.095)	15.575 (0.149)
1154+186	LP 434-97	15.15	15.03	15.02	15.098 (0.042)	15.220 (0.099)	15.087 (0.145)
1208+576	LHS 2522	14.64	14.39	14.32	14.679 (0.034)	14.362 (0.052)	14.458 (0.095)
1236-495	LTT 4816	13.92	13.90	13.98	13.806 (0.024)	13.815 (0.036)	13.907 (0.062)
1239+454	LHS 2596	15.47	15.30	15.30	15.599 (0.062)	15.197 (0.101)	15.727 (null)
1244+149	G61-17	15.84	15.86	15.84	15.802 (0.067)	15.627 (0.136)	15.721 (0.217)

Table 1—Continued

WD	Name	J_{CIT}	H_{CIT}	K_{CIT}	$J_{2\text{MASS}} (\sigma_J)$	$H_{2\text{MASS}} (\sigma_H)$	$K_{S2\text{MASS}} (\sigma_K)$
1247+550	LP 131-66	15.72	15.67	15.63	15.795 (0.067)	15.659 (0.131)	15.396 (0.212)
1257+037	LHS 2661	14.56	14.33	14.25	14.655 (0.040)	14.316 (0.050)	14.220 (0.089)
1257+278	G149-28	14.99	14.91	14.91:	15.132 (0.046)	14.977 (0.076)	14.986 (0.089)
1300+263	LHS 2673	16.89	16.71	16.70	16.801 (0.142)	16.399 (0.214)	16.436 (null)
1310–472	ER 8	15.21	15.11	15.03	15.135 (0.045)	15.045 (0.080)	14.735 (0.123)
1313–198	LHS 2710	15.87	15.70	15.56	15.875 (0.082)	15.612 (0.097)	15.550 (0.190)
1325+581	G199-71	15.82	15.68	15.65	15.945 (0.092)	15.700 (0.147)	15.716 (0.251)
1328+307	G165-7	15.50	15.36	15.34	15.402 (0.044)	15.282 (0.087)	15.413 (0.135)
1330+015	G62-46	16.38	16.25	16.17:	16.396 (0.119)	16.298 (0.206)	15.802 (null)
1334+039	Wolf 489	13.06	12.80	12.70	13.064 (0.024)	12.819 (0.026)	12.690 (0.021)
1344+106	LHS 2800	14.38	14.20	14.19	14.407 (0.038)	14.139 (0.053)	14.235 (0.080)
1345+238	LP 380-5	13.92	13.67	13.59	13.921 (0.027)	13.669 (0.036)	13.621 (0.040)
1346+121	LHS 2808	16.52	16.43	16.32	16.463 (0.118)	16.193 (0.242)	15.810 (null)
1418–088	G124-26	14.81	14.69	14.69	14.764 (0.037)	14.731 (0.057)	14.756 (0.103)
1444–174	LHS 378	14.94	14.79	14.68	14.948 (0.029)	14.640 (0.047)	14.724 (0.108)
1455+298	LHS 3007	14.86	14.73	14.72	14.972 (0.047)	14.606 (0.075)	14.739 (0.128)
1503–070	GD 175	15.07	14.93	14.91	15.079 (0.052)	14.988 (0.100)	14.847 (0.104)
1602+010	LHS 3151	16.08	15.86	15.67	16.078 (0.081)	15.969 (0.173)	15.526 (0.176)
1606+422	Case 2	13.92	13.92	14.01	13.984 (0.025)	14.026 (0.042)	14.050 (0.073)
1609+135	LHS 3163	14.77	14.76	14.75	14.861 (0.036)	14.779 (0.056)	14.857 (0.109)
1625+093	G138-31	15.34	15.12	15.06	15.250 (0.062)	15.187 (0.103)	15.036 (0.142)
1626+368	Ross 640	13.58	13.57	13.58	13.637 (0.024)	13.652 (0.034)	13.575 (0.042)
1633+433	G180-63	13.95	13.76	13.73	13.991 (0.029)	13.773 (0.035)	13.607 (0.043)
1635+137	G138-47	16.11	15.96	15.98:	15.929 (0.076)	15.673 (0.144)	15.727 (0.211)
1637+335	G180-65	14.56	14.50	14.54	14.551 (0.031)	14.467 (0.045)	14.424 (0.081)
1639+537	GD 356	14.54	14.46	14.42	14.493 (0.027)	14.479 (0.048)	14.369 (0.085)
1655+215	LHS 3254	13.89	13.80	13.85	13.886 (0.026)	13.816 (0.030)	13.863 (0.050)
1705+030	G139-13	14.62	14.50	14.48	14.565 (0.032)	14.499 (0.032)	14.511 (0.078)
1716+020	G19-20	14.68	14.65	14.71:	14.603 (0.056)	14.534 (0.070)	14.562 (0.109)
1733–544	L270-137	14.89	14.55	14.46	14.802 (0.044)	14.677 (0.084)	14.693 (0.105)
1736+052	G140-2	15.62	15.56	15.49	15.682 (0.067)	15.573 (0.122)	15.351 (0.175)
1748+708	G240-72	12.77	12.70	12.50	12.709 (0.021)	12.528 (0.023)	12.507 (0.023)
1811+327A	G206-17	15.71	15.56	15.54	15.716 (0.057)	15.675 (0.126)	15.760 (0.201)
1811+327B	G206-18	16.08	15.94	15.82:	16.214 (0.091)	15.953 (0.172)	15.809 (0.213)
1818+126	G141-2	15.07	14.90	14.87	14.989 (0.040)	14.885 (0.069)	14.876 (0.108)
1820+609	G227-28	13.96	13.73	13.65	14.075 (0.032)	13.810 (0.030)	13.797 (0.052)
1824+040	G21-15	14.07	14.14	14.14	14.107 (0.032)	14.111 (0.045)	14.225 (0.084)
1829+547	G227-35	14.76	14.61	14.50	14.803 (0.045)	14.478 (0.053)	14.505 (0.078)
1831+197	G184-12	15.93	15.82	15.81	15.977 (0.095)	16.043 (0.184)	15.608 (0.198)
1840+042	GD 215	14.53:	14.46:	14.50:	14.443 (0.050)	14.374 (0.075)	14.651 (0.099)
1855+338	G207-9	14.74	14.72	14.77	14.737 (0.034)	14.769 (0.056)	14.799 (0.124)
1917+386	G125-3	13.77	13.69	13.59	13.776 (0.030)	13.669 (0.032)	13.519 (0.025)
1953–011	LHS 3501	13.12	13.02	13.02	13.070 (0.029)	13.029 (0.031)	13.014 (0.040)
2002–110	LHS 483	15.32	15.11	15.09	15.276 (0.055)	14.995 (0.072)	14.746 (0.105)
2011+065	G24-9	14.94	14.79	14.75	15.021 (0.049)	14.878 (null)	15.090 (null)
2048+263	G187-8	14.12	13.83	13.79	14.100 (0.056)	13.908 (0.068)	13.602 (null)

Table 1—Continued

WD	Name	J_{CIT}	H_{CIT}	K_{CIT}	$J_{2\text{MASS}} (\sigma_J)$	$H_{2\text{MASS}} (\sigma_H)$	$K_{S2\text{MASS}} (\sigma_K)$
2054–050	vB 11	14.82	14.61	14.54	14.734 (0.081)	14.565 (0.134)	14.327 (0.136)
2059+190	G144-51	15.52	15.36	15.34	15.642 (0.070)	15.559 (0.141)	15.397 (0.159)
2059+247	G187-16	15.45	15.29	15.26	15.522 (0.057)	15.205 (0.082)	15.061 (0.143)
2059+316	G187-15	14.94	14.97	14.98	14.968 (0.053)	14.927 (0.068)	14.980 (0.115)
2105–820	L24-52	13.52	13.53	13.58	13.478 (0.026)	13.451 (0.033)	13.533 (0.039)
2107–216	LHS 3636	15.63	15.45:	15.40:	15.688 (0.055)	15.476 (0.106)	15.695 (0.214)
2111+261	G187-32	14.15	14.08	14.09	14.230 (0.036)	14.116 (0.041)	14.095 (0.057)
2136+229	G126-18	15.04	14.96	15.09	15.106 (0.060)	15.055 (0.087)	14.816 (0.116)
2140+207	LHS 3703	12.95	12.93	12.95	12.981 (0.021)	12.928 (0.035)	12.922 (0.029)
2207+142	G18-34	14.99	14.81	14.84	14.971 (0.040)	14.782 (0.086)	14.772 (0.098)
2246+223	G67-23	14.28	14.31	14.37	14.341 (0.029)	14.317 (0.047)	14.360 (0.090)
2248+293	G128-7	14.24	14.01	13.94	14.316 (0.029)	13.983 (0.038)	13.941 (0.044)
2251–070	LP 701-29	13.86	13.63	13.47	14.013 (0.026)	13.685 (0.036)	13.546 (0.053)
2253–081	G156-64	15.59	15.47	15.36:	15.629 (0.067)	15.279 (0.086)	15.195 (0.168)
2311–068	G157-34	14.98	14.93	14.90	14.951 (0.036)	14.942 (0.071)	14.730 (0.093)
2312–024	LHS 3917	15.70	15.53	15.58	15.488 (0.059)	15.754 (0.170)	14.862 (null)
2316–064	LHS 542	16.38	16.14	16.10	16.306 (0.092)	15.837 (0.139)	15.200 (null)
2323+157	GD 248	15.06	15.08	15.06	15.051 (0.043)	14.938 (0.072)	14.881 (0.138)
2329+267	G128-72	15.13	15.03	15.18	15.184 (0.041)	15.100 (0.087)	15.030 (0.111)
2345–447	ESO 292-43	16.66	16.59	16.33	16.517 (0.142)	16.360 (null)	16.332 (null)
2347+292	LHS 4019	14.59	14.35	14.24	14.571 (0.029)	14.345 (0.044)	14.159 (0.065)
2352+401	G171-27	14.57	14.52	14.50	14.576 (0.038)	14.453 (0.061)	14.508 (0.086)

Note. — Table 1 is available in its entirety in the electronic edition of the *Astrophysical Journal*. A portion is shown here for guidance regarding its form and content. CIT uncertainties are 5% except for the data marked “:” or “:.”, which indicate 10% and 20% uncertainties, respectively. 2MASS magnitudes with null uncertainties are lower limits.

Table 2. Statistical Comparison of CIT and 2MASS Magnitudes

Bandpass	No. of Stars	Mean	Standard Deviation	$\langle\sigma_{2\text{MASS}}\rangle$	$\langle\sigma\rangle^{\text{a}}$
$J_{\text{CIT}} - J_{2\text{MASS}}$	159	-0.0046	0.0805	0.0502	0.0745
$H_{\text{CIT}} - H_{2\text{MASS}}$	157	+0.0180	0.1126	0.0807	0.0997
$K_{\text{CIT}} - K_{S\ 2\text{MASS}}$	143	+0.0247	0.1561	0.1096	0.1253
$J_{\text{CIT}} - J_{2\text{MASS}}$ (S/N > 10)	130	-0.0083	0.0679	0.0409	0.0662
$H_{\text{CIT}} - H_{2\text{MASS}}$ (S/N > 10)	97	+0.0094	0.0675	0.0502	0.0726
$K_{\text{CIT}} - K_{S\ 2\text{MASS}}$ (S/N > 10)	49	+0.0133	0.0692	0.0466	0.0697

^aAverage value of σ where for a single star, $\sigma = (\sigma_{2\text{MASS}}^2 + \sigma_{\text{CIT}}^2)^{1/2}$.

Table 3. Sample of White Dwarfs with Predicted NIR Photometry

WD	T_{eff} (K)	$\log g$	V	J_{pred}	H_{pred}	$K_{S \text{ pred}}$	$J_{2\text{MASS}} (\sigma_J)$	$H_{2\text{MASS}} (\sigma_H)$	$K_{S 2\text{MASS}} (\sigma_K)$
0023+388	10785	8.14	15.97	15.988	15.979	16.121	13.810 (0.026)	13.268 (0.030)	12.939 (0.033)
0034–211	17217:	8.04:	14.53	14.934	15.000	15.161	11.454 (0.023)	10.884 (0.021)	10.648 (0.026)
0131–163	49042	7.81	13.96	14.667	14.808	15.000	12.966 (0.027)	12.468 (0.028)	12.215 (0.030)
0145–257	25635	7.97	14.51	15.089	15.200	15.382	12.412 (0.026)	11.830 (0.021)	11.594 (0.023)
0145–221	11549	8.14	14.85	14.965	14.974	15.122	14.923 (0.032)	14.450 (0.045)	14.335 (0.064)
0205+133	58692	7.63	15.30	16.009	16.152	16.342	12.799 (0.022)	12.198 (0.024)	11.961 (0.020)
0303–007	18700	7.97	16.00	16.439	16.517	16.679	13.164 (0.024)	12.627 (0.027)	12.405 (0.026)
0347–137	12621	8.19	14.00	14.205	14.230	14.380	12.080 (0.029)	11.540 (0.029)	11.296 (0.023)
0353+284	31000:	7.90:	11.70	12.350	12.479	12.672	9.843 (0.023)	9.275 (0.024)	9.057 (0.017)
0429+176	13600	8.56	13.93	14.188	14.214	14.372	10.753 (0.021)	10.161 (0.019)	9.913 (0.017)
0430+136	35976	7.90	16.45	17.126	17.263	17.456	13.533 (0.021)	12.877 (0.023)	12.634 (0.026)
0628–020	6912	8.15	15.33	14.509	14.311	14.371	10.729 (0.027)	10.144 (0.026)	9.857 (0.024)
0710+741	10119	8.11	14.97	14.881	14.851	14.986	14.692 (0.033)	14.423 (0.061)	14.148 (0.065)
0812+478	60923	7.58	15.22	15.931	16.074	16.264	14.587 (0.032)	14.165 (0.041)	13.882 (0.047)
0915+201	69970	7.33	16.64	17.354	17.498	17.687	15.721 (0.058)	15.166 (0.078)	14.867 (0.080)
0950+139	94402	9.18	16.03	16.771	16.921	17.117	16.518 (0.097)	15.945 (0.157)	16.099 (0.258)
1001+203	21492	7.97	15.35	15.849	15.944	16.110	12.640 (0.021)	12.028 (0.021)	11.766 (0.020)
1013–050	60265	7.93	14.18	14.893	15.037	15.228	10.607 (0.027)	9.990 (0.025)	9.770 (0.023)
1026+002	17183	7.97	13.60	14.001	14.068	14.228	11.751 (0.024)	11.219 (0.027)	10.943 (0.021)
1037+512	20099	8.03	16.25	16.721	16.809	16.971	13.796 (0.024)	13.261 (0.026)	12.972 (0.026)
1108+325	62950	7.59	16.80	17.512	17.656	17.845	15.802 (0.072)	15.188 (0.079)	15.228 (0.179)
1123+189	51682	7.86	14.16	14.865	15.007	15.198	12.754 (0.023)	12.217 (0.019)	11.990 (0.020)
1210+464	27667	7.85	15.79	16.400	16.520	16.707	12.035 (0.023)	11.396 (0.021)	11.161 (0.020)
1218+497	35656	7.87	16.24	16.915	17.051	17.244	14.588 (0.038)	14.002 (0.036)	13.837 (0.060)
1224+309	28824	7.38	16.10	16.720	16.846	17.034	15.129 (0.048)	14.669 (0.068)	14.393 (0.077)
1339+346	15959	7.82	15.87	16.225	16.287	16.441	14.094 (0.027)	13.700 (0.031)	13.591 (0.036)
1434+289	32795	8.00	15.75	16.413	16.546	16.739	16.514 (0.119)	16.330 (0.203)	15.924 (0.293)
1435+370	15268	7.99	16.00	16.336	16.389	16.543	13.457 (0.024)	12.965 (0.025)	12.746 (0.028)
1443+337	29763	7.83	16.39	17.027	17.154	17.345	14.284 (0.030)	13.725 (0.030)	13.516 (0.040)
1458+171	21945	7.43	16.30	16.800	16.900	17.065	14.701 (0.031)	14.209 (0.045)	13.847 (0.047)
1502+349	21339	7.96	15.78	16.276	16.371	16.535	15.231 (0.045)	14.766 (0.061)	14.314 (0.067)
1504+546	24689	7.86	16.00	16.560	16.668	16.845	13.847 (0.025)	13.260 (0.026)	13.001 (0.027)
1517+501	31100:	7.84:	17.46	18.110	18.240	18.432	15.559 (0.060)	14.746 (0.071)	14.157 (0.072)
1610+383	14450	7.83	16.40	16.701	16.749	16.898	14.437 (0.034)	13.807 (0.036)	13.521 (0.042)
1619+525	18041	7.90	15.81	16.232	16.306	16.467	14.168 (0.032)	13.545 (0.035)	13.425 (0.042)
1619+414	14091	7.93	16.80	17.087	17.129	17.279	13.937 (0.021)	13.311 (0.029)	13.025 (0.027)
1622+323	68277	7.56	16.33	17.045	17.189	17.379	14.633 (0.029)	13.963 (0.031)	13.773 (0.039)
1631+781	44931	7.76	13.38	14.076	14.216	14.408	10.975 (0.021)	10.398 (0.021)	10.164 (0.014)
1639+153	7482	8.42	15.70	15.032	14.869	14.948	15.073 (0.042)	14.979 (0.087)	15.060 (0.128)
1643+143	26849	7.91	15.64	16.239	16.355	16.540	12.732 (0.024)	12.125 (0.031)	11.957 (0.024)
1711+668	53751	8.47	17.00	17.711	17.854	18.048	15.120 (0.043)	14.457 (0.057)	14.211 (0.087)
1717–345	12700:	7.75:	16.38	16.588	16.620	16.762	12.870 (0.039)	12.208 (0.060)	11.940 (0.054)
2151–015	9137	8.21	14.41	14.122	14.049	14.168	12.452 (0.029)	11.778 (0.022)	11.414 (0.027)
2256+249	22151	7.82	13.64	14.150	14.249	14.416	11.675 (0.020)	11.180 (0.025)	10.915 (0.018)
2257+162	27556	8.33	16.14	16.756	16.873	17.061	15.439 (0.054)	15.088 (0.074)	14.736 (0.108)
2317+268	31460	7.70	16.30	16.951	17.082	17.275	14.609 (0.033)	14.074 (0.036)	13.783 (0.050)

Table 3—Continued

WD	T_{eff} (K)	$\log g$	V	J_{pred}	H_{pred}	$K_{S \text{ pred}}$	$J_{2\text{MASS}} (\sigma_J)$	$H_{2\text{MASS}} (\sigma_H)$	$K_{S 2\text{MASS}} (\sigma_K)$
2336–187	7882	7.82	15.60	15.035	14.896	14.987	15.057 (0.040)	14.939 (0.063)	14.681 (0.093)

Note. — Uncertainties of the atmospheric parameters are 1.2% in T_{eff} and 0.038 dex in $\log g$. The V magnitudes are from various sources in the literature. The objects marked with a colon are contaminated by the companion in the visible and the uncertainties are correspondingly larger.

Table 4. Sample of Massive White Dwarfs

WD	T_{eff} (K)	M/M_{\odot}	V	J_{pred}	H_{pred}	K_{pred}	$J_{2\text{MASS}} (\sigma_J)$	$H_{2\text{MASS}} (\sigma_H)$	$K_{S2\text{MASS}} (\sigma_K)$
0033+016	10984	1.11	15.61	15.638	15.632	15.679	15.650 (0.057)	15.522 (0.090)	16.119 (0.303)
0052+226	9652	1.05	16.16	15.966	15.918	15.947	16.021 (0.077)	16.109 (0.162)	15.522 (0.212)
0052–147	25683	0.80	15.12	15.715	15.832	15.912	15.724 (0.061)	15.532 (0.109)	15.457 (null)
0101+059	14191	0.83	–	–	–	–	16.214 (0.089)	16.387 (0.210)	17.182 (null)
0143+216	9292	0.92	15.05	14.792	14.732	14.755	14.784 (0.036)	14.812 (0.060)	14.676 (0.077)
0213+396	9323	0.96	14.54	14.287	14.227	14.250	14.304 (0.030)	14.223 (0.052)	14.144 (0.049)
0231–054	13552	1.02	14.28	14.545	14.583	14.643	14.540 (0.033)	14.558 (0.052)	14.659 (0.101)
0232+525	16738	0.80	13.75	14.150	14.220	14.283	14.218 (0.031)	14.261 (0.053)	14.497 (0.072)
0346–011	41185	1.27	14.01	14.728	14.867	14.957	14.747 (0.030)	14.863 (0.038)	15.120 (0.138)
0429+176	13600	0.97	13.93	14.192	14.231	14.290	10.753 (0.021)	10.161 (0.019)	9.913 (0.017)
0532–560	11556	0.92	16.00	16.110	16.125	16.176	16.023 (0.085)	15.882 (0.185)	16.348 (null)
0558+165	16199	0.81	15.69	16.071	16.137	16.199	16.004 (0.069)	16.189 (0.161)	15.605 (null)
0644+025	7242	1.00	15.71	14.990	14.820	14.793	14.868 (0.045)	14.757 (0.069)	14.576 (0.103)
0701–587	13696	0.91	14.46	14.731	14.773	14.831	14.844 (0.035)	14.856 (0.074)	15.067 (0.150)
0730+487	14311	0.91	14.96	15.264	15.311	15.370	15.143 (0.045)	15.191 (0.094)	15.395 (0.171)
0743+442	14501	0.84	14.87	15.183	15.234	15.292	15.230 (0.045)	15.403 (0.104)	15.179 (0.131)
0827+328	7508	0.96	15.73	15.077	14.921	14.903	14.985 (0.044)	14.964 (0.076)	14.865 (0.121)
0930+294	8362	0.98	15.98	15.525	15.416	15.420	15.588 (0.066)	15.399 (0.106)	15.284 (0.150)
0947+325	22055	0.82	15.43	15.957	16.060	16.126	16.011 (0.073)	16.127 (0.171)	16.503 (null)
0950+139	94402	1.36	16.03	16.789	16.939	17.029	16.518 (0.097)	15.945 (0.157)	16.099 (0.258)
1038+633	24447	0.86	15.15	15.725	15.836	15.912	15.723 (0.080)	15.748 (0.188)	15.389 (null)
1049–158	18989	0.83	14.36	14.820	14.907	14.970	14.789 (0.047)	14.818 (0.060)	15.116 (0.164)
1052+273	23103	0.86	14.12	14.664	14.771	14.841	14.619 (0.029)	14.674 (0.048)	14.784 (0.076)
1058–129	24311	1.06	15.75	16.328	16.437	16.513	15.520 (0.054)	15.689 (0.118)	15.437 (0.219)
1102+748	19712	0.84	14.97	15.448	15.539	15.601	15.556 (0.059)	15.487 (0.116)	15.552 (0.228)
1120+439	26950	0.85	15.81	16.428	16.549	16.632	16.053 (0.077)	15.977 (0.158)	16.200 (0.362)
1134+300	21276	0.96	12.52	13.036	13.134	13.199	12.993 (0.024)	13.105 (0.031)	13.183 (0.028)
1159–098	9536	1.10	15.90	15.682	15.628	15.654	15.555 (0.056)	15.480 (0.091)	15.384 (0.186)
1236–495	11748	1.10	13.80	13.923	13.935	13.989	13.806 (0.024)	13.815 (0.036)	13.907 (0.062)
1237–028	10236	0.97	15.97	15.888	15.865	15.903	15.971 (0.068)	15.922 (0.138)	15.754 (0.250)
1257+278	8733	0.81	15.41	15.040	14.954	14.966	15.132 (0.046)	14.977 (0.076)	14.986 (0.089)
1304+227	10444	0.87	–	–	–	–	16.413 (0.112)	16.601 (0.288)	16.498 (null)
1310+583	10555	0.80	14.09	14.070	14.063	14.106	14.016 (0.028)	14.004 (0.045)	14.081 (0.073)
1334–160	18667	0.80	15.34	15.792	15.876	15.939	15.532 (0.053)	15.553 (0.103)	15.733 (0.295)
1446+286	22891	0.89	14.54	15.086	15.192	15.261	15.172 (0.044)	15.269 (0.113)	15.537 (0.251)
1452+553	27636	0.82	–	–	–	–	16.642 (0.118)	16.606 (0.235)	16.720 (null)
1459+347	21516	0.92	15.74	16.259	16.359	16.424	16.402 (0.101)	16.327 (0.207)	15.645 (null)
1515+668	10317	0.86	15.33	15.268	15.251	15.291	15.295 (0.053)	15.240 (0.112)	15.180 (0.198)
1525+257	22291	0.80	15.65	16.181	16.286	16.352	16.258 (0.098)	16.101 (0.177)	16.022 (null)
1531–022	18617	0.88	14.00	14.453	14.535	14.600	14.395 (0.040)	14.484 (0.053)	14.618 (0.101)
1554+322	30497	0.85	–	–	–	–	16.561 (0.115)	17.617 (null)	16.016 (0.241)
1609+135	9321	1.01	15.11	14.854	14.793	14.816	14.861 (0.036)	14.779 (0.056)	14.857 (0.109)
1625+093	6870	0.88	16.14	15.318	15.125	15.086	15.250 (0.062)	15.187 (0.103)	15.036 (0.142)
1636+057	8537	1.07	16.46	16.040	15.941	15.948	16.057 (0.081)	15.897 (0.147)	15.919 (null)
1639+153	7482	0.86	15.68	15.021	14.863	14.844	15.073 (0.042)	14.979 (0.087)	15.060 (0.128)
1647+591	12258	0.81	12.23	12.412	12.444	12.497	12.425 (0.021)	12.463 (0.021)	12.522 (0.030)

Table 4—Continued

WD	T_{eff} (K)	M/M_{\odot}	V	J_{pred}	H_{pred}	K_{pred}	$J_{2\text{MASS}} (\sigma_J)$	$H_{2\text{MASS}} (\sigma_H)$	$K_{S2\text{MASS}} (\sigma_K)$
1711+668	53751	0.96	17.00	17.728	17.872	17.960	15.120 (0.043)	14.457 (0.057)	14.211 (0.087)
1840+042	8925	0.81	14.79	14.461	14.384	14.400	14.443 (0.050)	14.374 (0.075)	14.651 (0.099)
1855+338	11958	0.83	14.64	14.795	14.820	14.874	14.737 (0.034)	14.769 (0.056)	14.799 (0.124)
2039–682	15855	0.89	13.41	13.781	13.842	13.904	13.729 (0.026)	13.806 (0.039)	13.800 (0.050)
2051–208	20512	1.23	15.06	15.570	15.659	15.725	15.590 (0.050)	15.669 (0.112)	15.839 (0.226)
2059+190	6980	0.86	16.38	15.589	15.402	15.366	15.642 (0.070)	15.559 (0.141)	15.397 (0.159)
2124+550	13341	0.82	14.70	14.952	14.993	15.049	14.987 (0.053)	14.957 (0.090)	14.905 (0.162)
2205–139	25263	0.81	15.08	15.668	15.783	15.861	15.648 (0.067)	15.610 (0.114)	15.582 (0.217)
2220+133	22675	0.88	15.60	16.141	16.246	16.315	16.264 (0.112)	16.046 (0.180)	15.367 (null)
2246+223	10647	1.10	14.39	14.368	14.354	14.397	14.341 (0.029)	14.317 (0.047)	14.360 (0.090)
2313+682	8977	0.83	16.18	15.861	15.787	15.804	15.908 (0.098)	15.766 (0.175)	15.387 (0.210)

Note. — 2MASS magnitudes with null uncertainties are lower limits. Mean uncertainties of effective temperatures and masses are 1.2% and 0.03 M_{\odot} , respectively.

Fig. 1.— Differences in magnitudes between the infrared CIT and 2MASS photometric systems for each individual filter as a function of the 2MASS magnitude for our common sample of 160 cool white dwarfs. The error bars represent the combined quadratic uncertainties of both photometric data sets. The horizontal dotted lines indicate the mean magnitude differences between both data sets. Objects located on the left side of the vertical dotted lines meet the PSC level 1 requirements ($S/N > 10$), which correspond to $J < 15.8$, $H < 15.1$, and $K_S < 14.3$. The ten objects represented by open circles are discussed in the text and in Figure 3.

Fig. 2.— *Top:* $(J - H)$ vs. $(H - K/K_S)$ two-color diagrams for 143 cool white dwarfs taken from Table 1 and detected by 2MASS in all three bands. The left and right panels correspond to the CIT and 2MASS magnitudes, respectively. The error bars indicate the mean uncertainties of each data set. *Bottom:* Same as the top panels but for the 49 white dwarfs satisfying the level 1 requirements. The region above the dashed line and that defined by the dotted rectangle correspond to the color criteria defined by Wachter et al. (2003) for selecting binary candidates and tentative binary candidates, respectively. The ten objects shown by open circles are discussed in the text and in Figure 3.

Fig. 3.— Fits to the optical $BVRI$ and infrared JHK CIT photometric energy distributions (*thin error bars*) for ten objects from our cool white dwarf sample. The atmospheric parameters obtained from a fit to the observed energy distribution are given in each panel and the corresponding monochromatic model fluxes are shown by the solid line. For clarity, we do not plot the model fluxes averaged over the filter bandpasses and used in the fitting procedure as they coincide almost perfectly with the monochromatic fluxes. Also shown by thick error bars are the corresponding 2MASS fluxes.

Fig. 4.— Same as Figure 2 but with the four regions defined by Wellhouse et al. (2005, see text). The filled and open circles correspond to the CIT and 2MASS colors, respectively. The two objects with CIT data labeled in the figure and discussed in the text are (1) 1748+708 and (2) 2251–070.

Fig. 5.— Observed 2MASS fluxes (*error bars*) for several binary and tentative binary candidates from Wachter et al. (2003) compared with the predictions of model atmospheres (*solid lines*) normalized at V . The atmospheric parameters derived from the spectroscopic method are given in each panel.

Fig. 6.— Fits to the energy distribution of white dwarfs from the sample of Kilic et al. (2006b). The observed $BVRI$ and JHK (CIT) fluxes along with the 4.5 and 8 μm *Spitzer* fluxes are shown by error bars. The flux scale is logarithmic and each star is shifted vertically

by a constant for clarity. The model monochromatic fluxes are shown by solid lines while the fluxes averaged over the filter bandpasses are indicated by filled and open circles for pure hydrogen and pure helium atmospheric compositions, respectively.

Fig. 7.— The ratio of observed to predicted *Spitzer* fluxes for 12 objects from the sample of Kilic et al. (2006b) as a function of effective temperature. The predicted fluxes and T_{eff} values are obtained from simultaneous fits to the *BVRIJHK* and 4.5 and 8 μm photometric data. For Ross 627 (1121+216), only the *Spitzer* 4.5 μm flux is used since the 8 μm flux is affected by a nearby star.

Fig. 8.— Same as Fig. 5 but for the five white dwarfs discussed in § 5.

Fig. 9.— Differences between the 2MASS observed and predicted ($J - H$) and ($J - K_s$) color indices for our sample of massive white dwarfs (Table 4) as a function of H and K_s , respectively. In the upper panel, 53 objects are detected at both J and H , while in the lower panel 42 objects are detected at both J and K_s . The uncertainties are from the 2MASS PSC. Known white dwarfs (not necessarily massive) with a circumstellar disk are shown by triangles and correspond to (A) G29-38, (B) GD 362 and (C) GD 56; the observed colors for G29-38 and GD 56 are from 2MASS and for GD 362 from Becklin et al. (2005). Also identified in the figure and discussed in the text are (1) G1-7 and (2) CBS 413. Left of the dotted vertical lines are objects for which the 2MASS level-1 requirements are satisfied for the corresponding color index. The horizontal dotted lines represent identical values of observed and theoretical color indices.

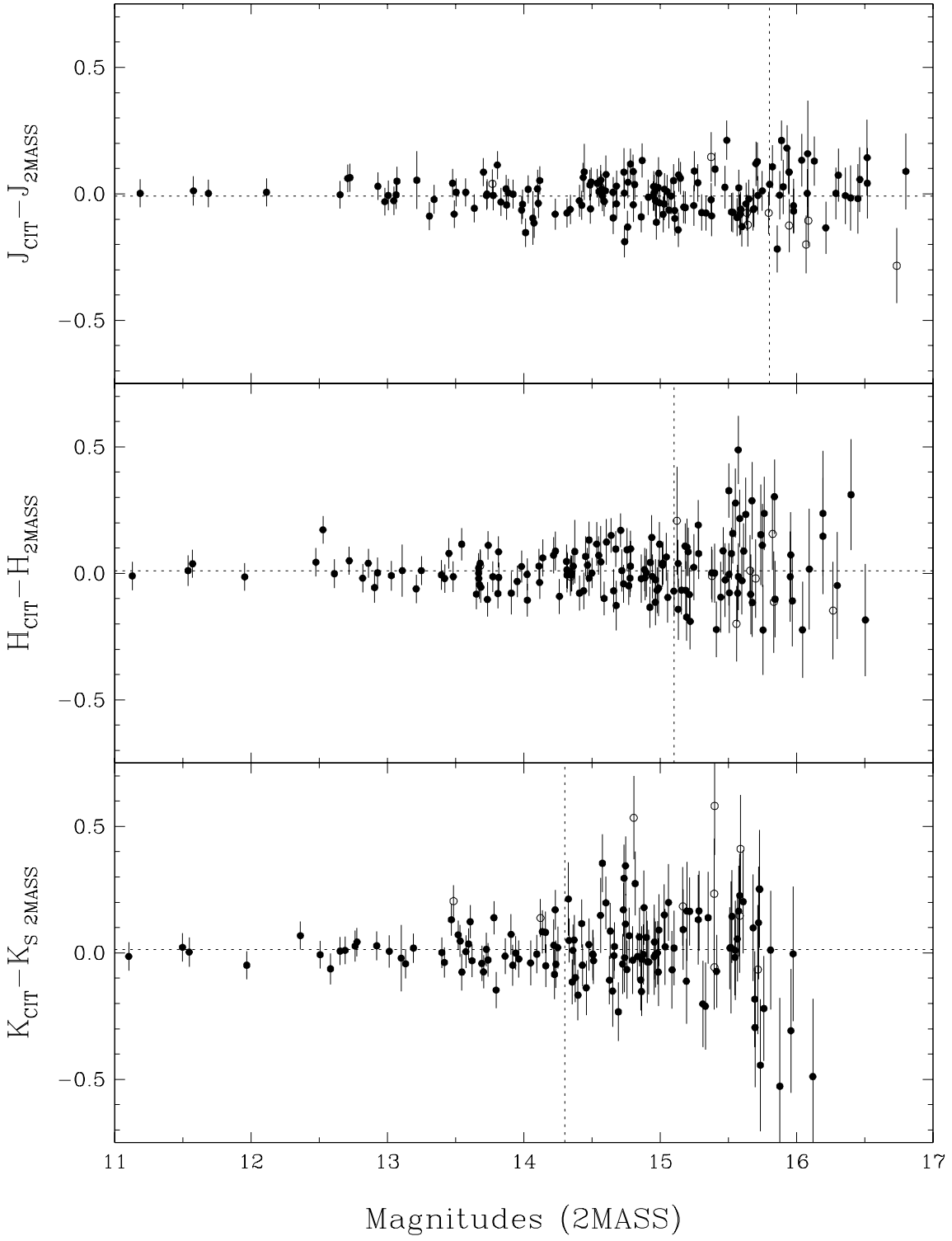


Figure 1

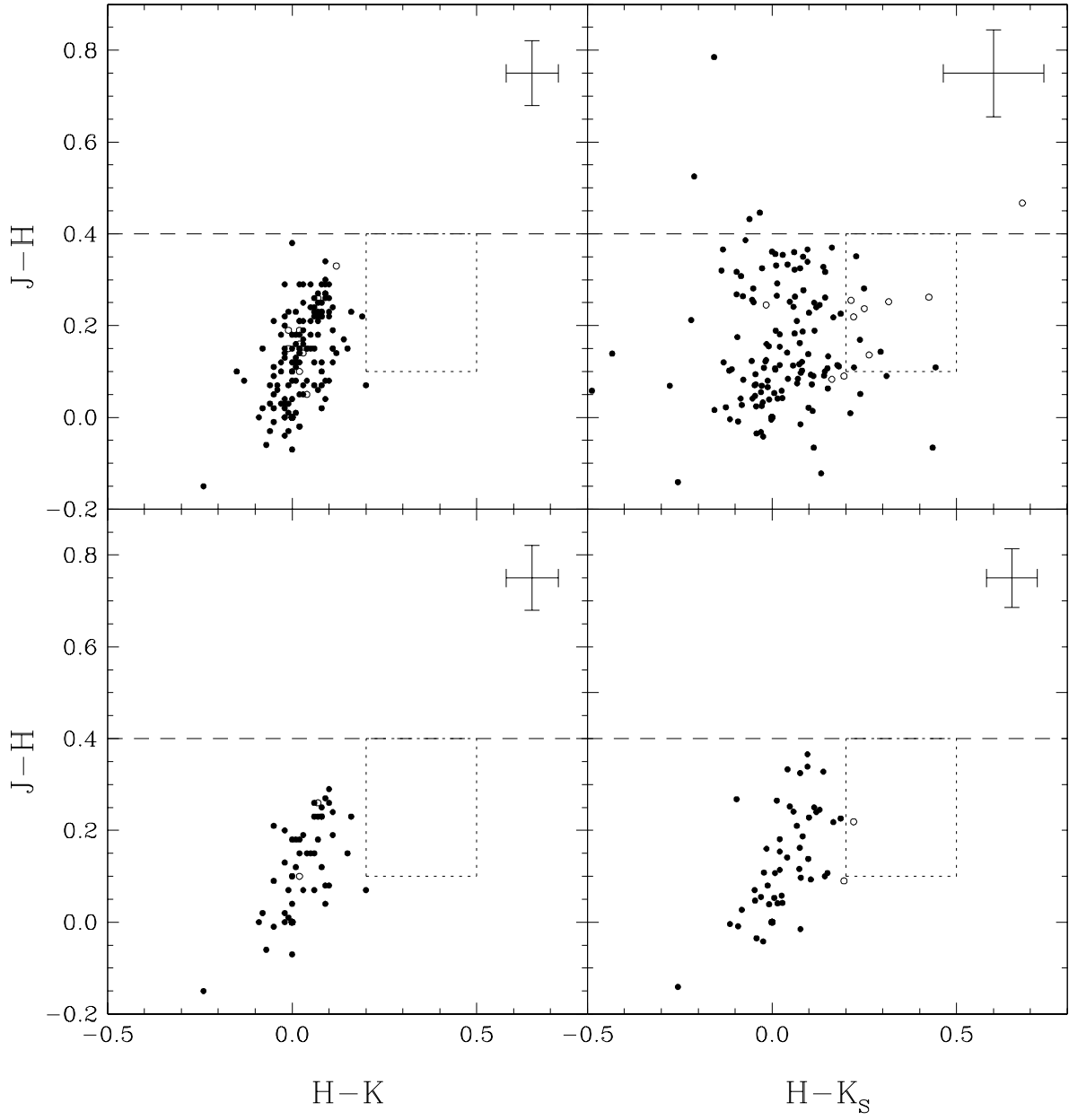


Figure 2

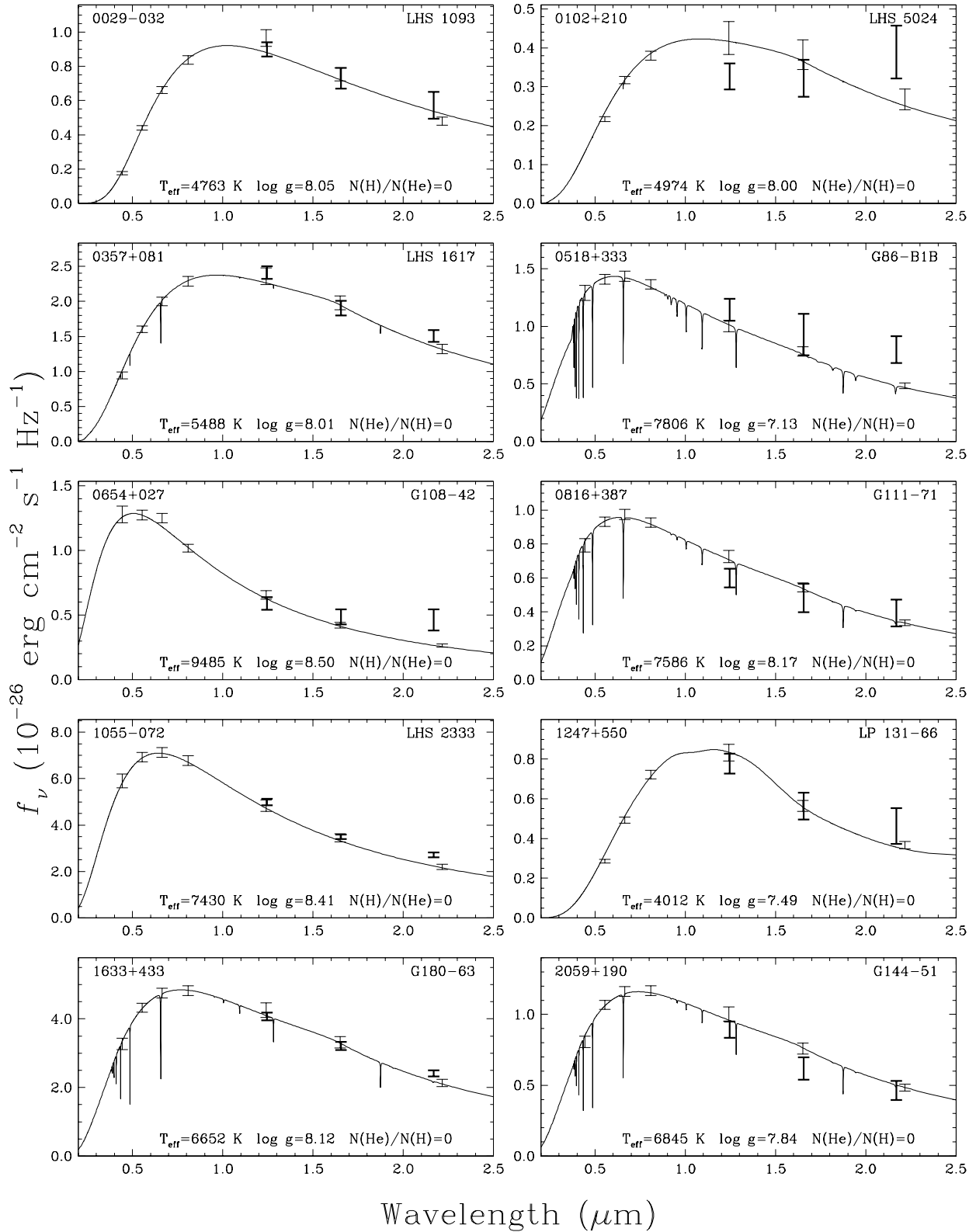


Figure 3

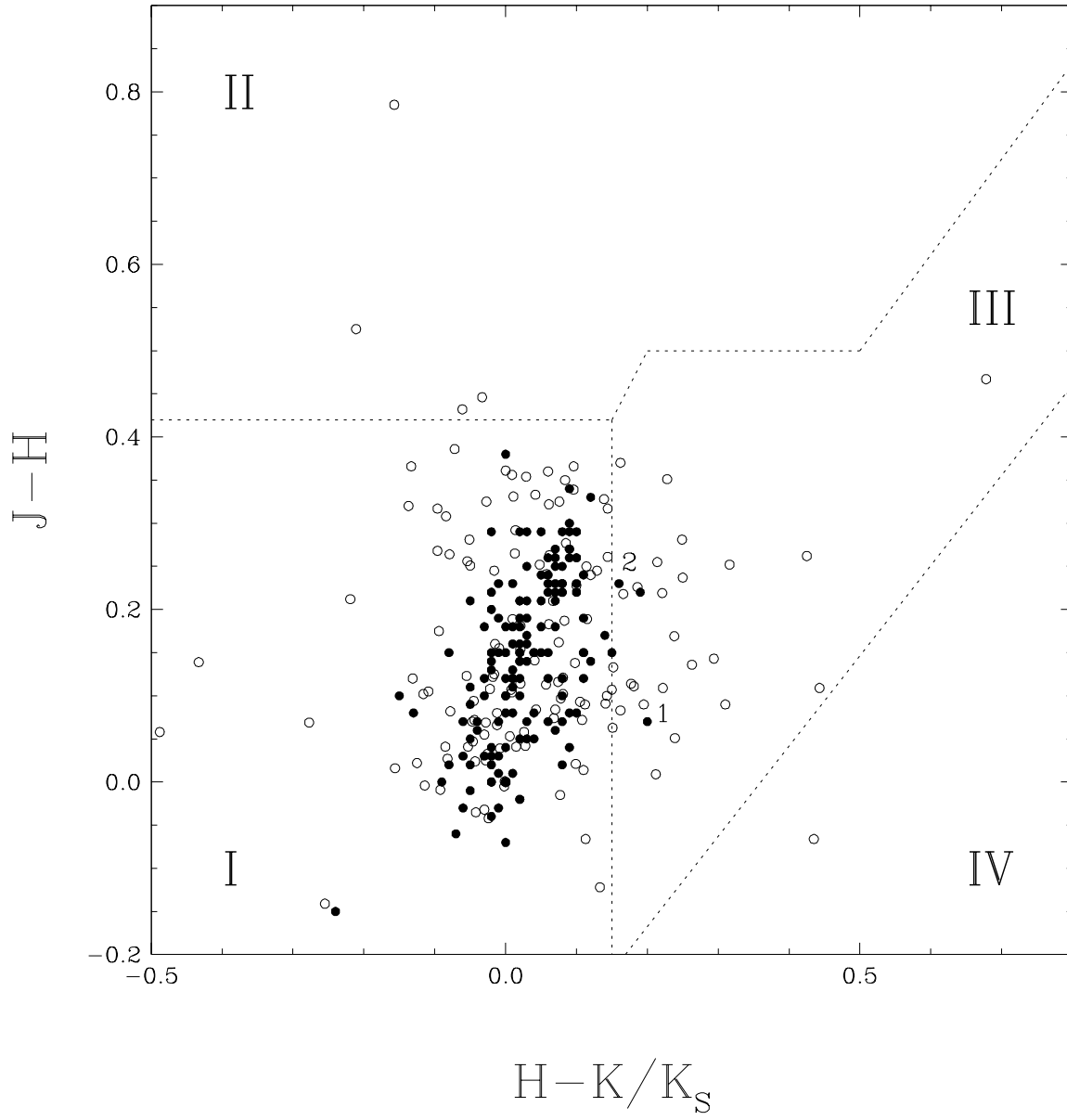


Figure 4

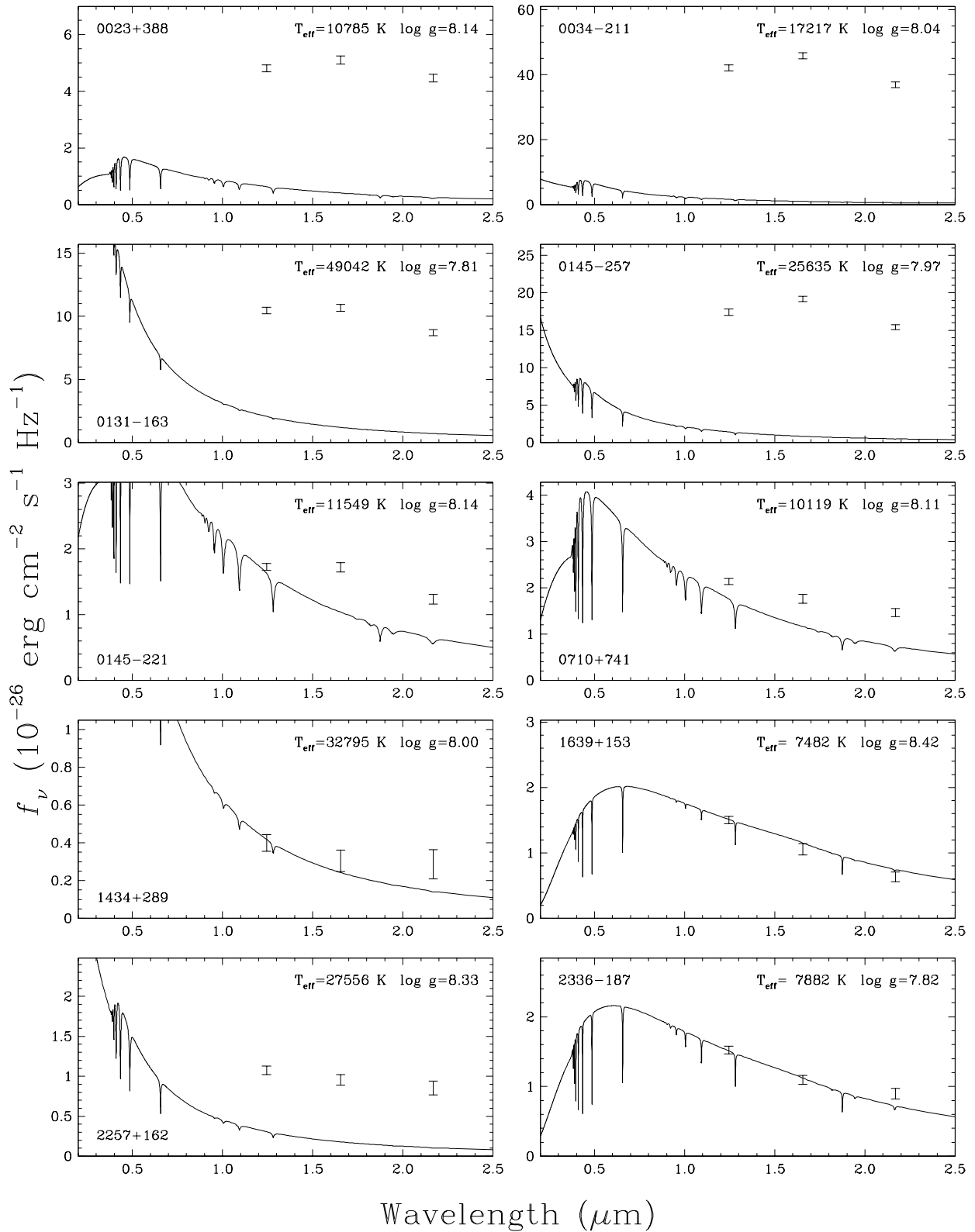


Figure 5

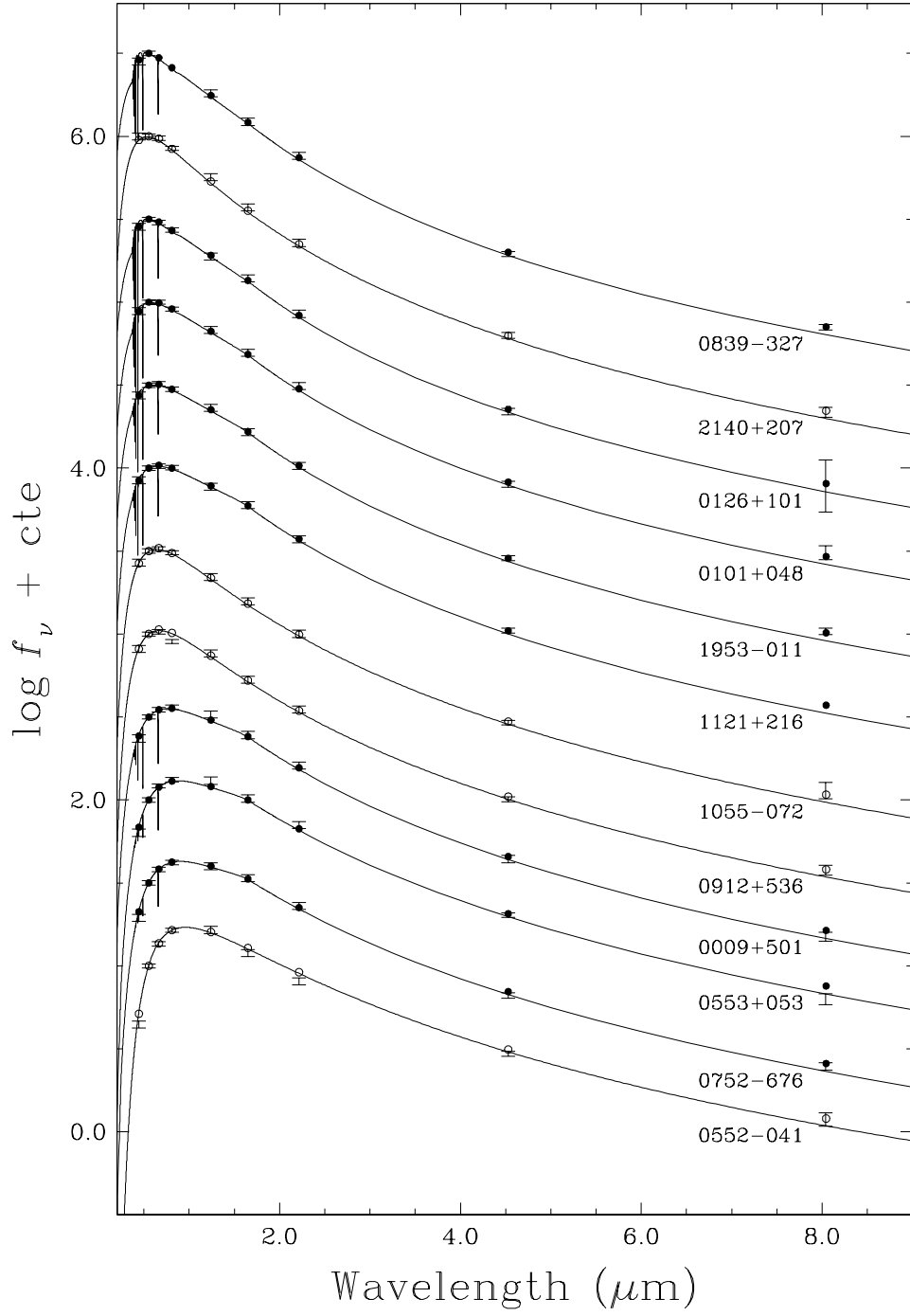


Figure 6

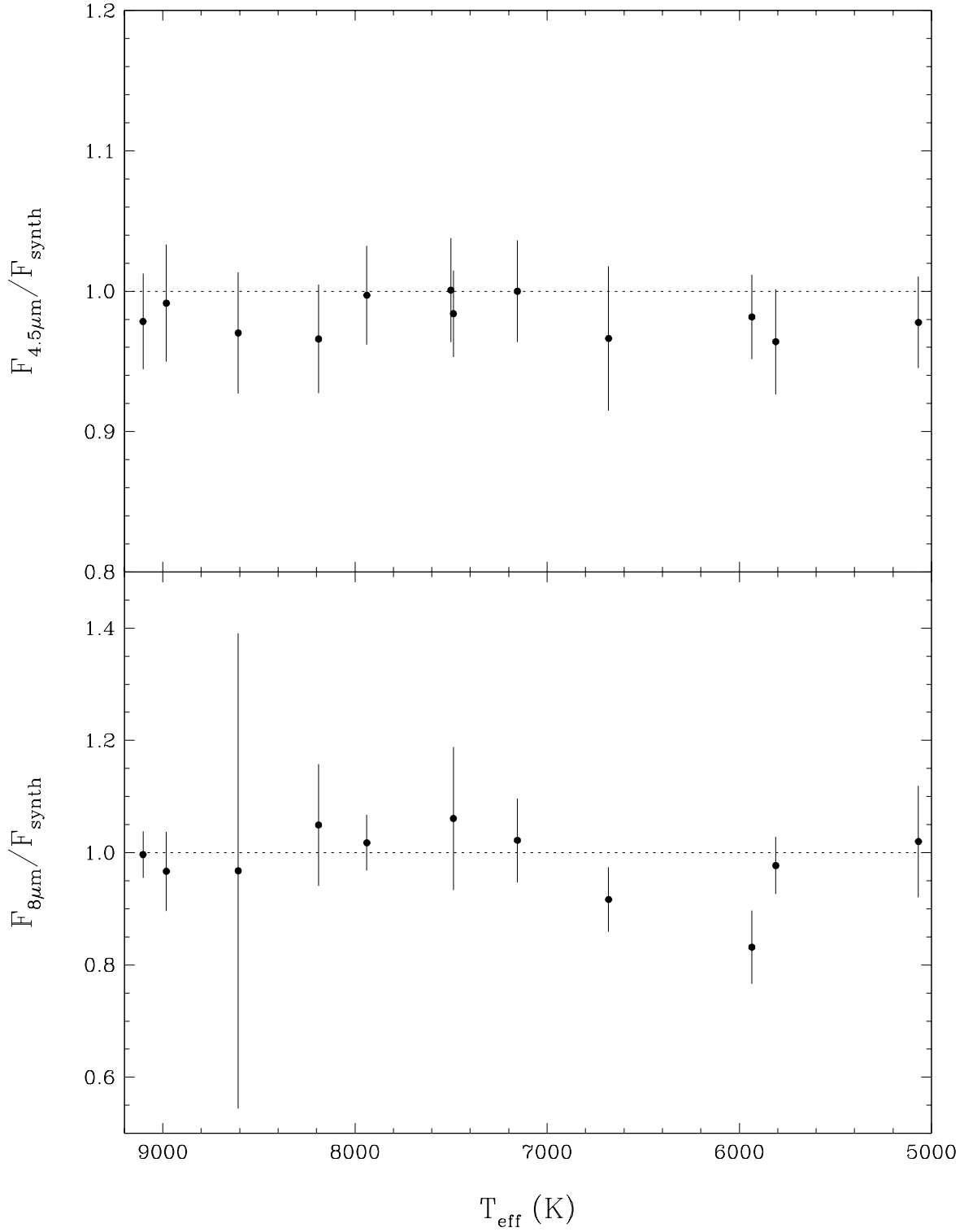


Figure 7

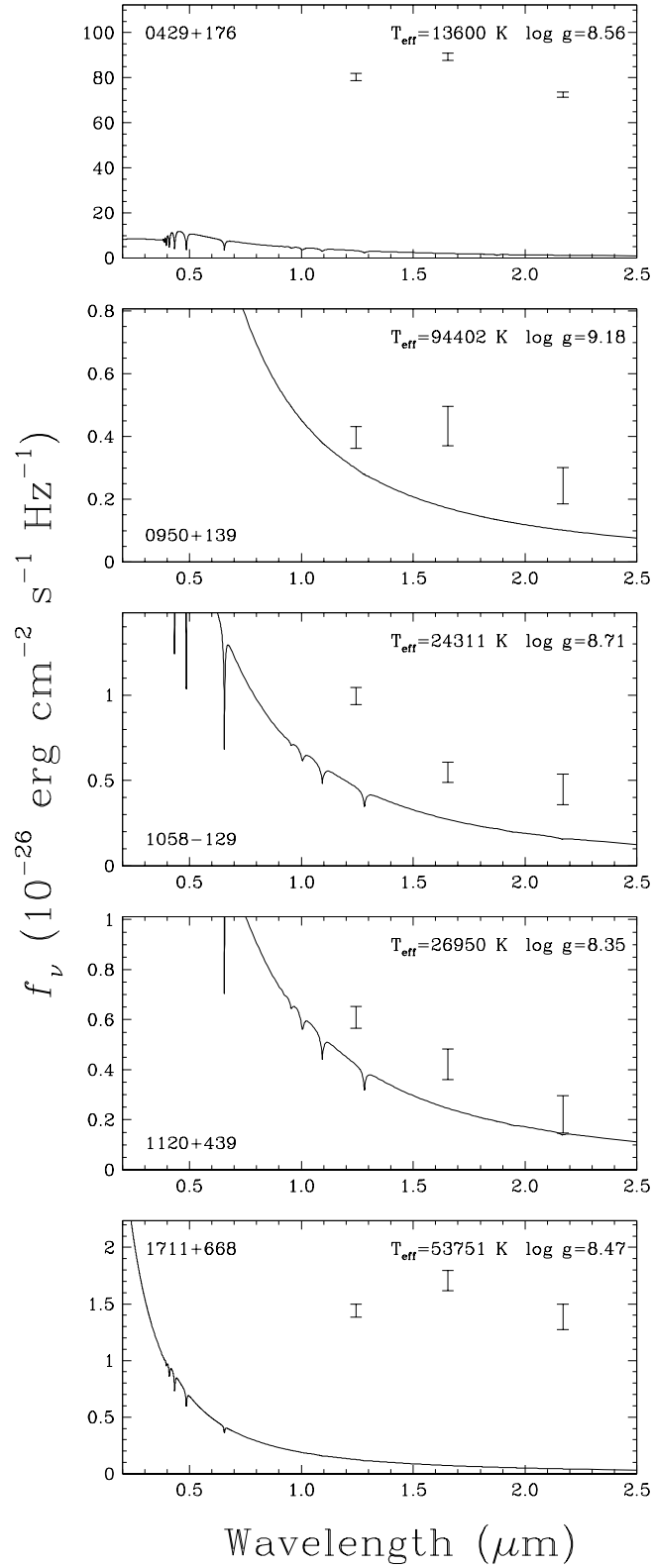


Figure 8

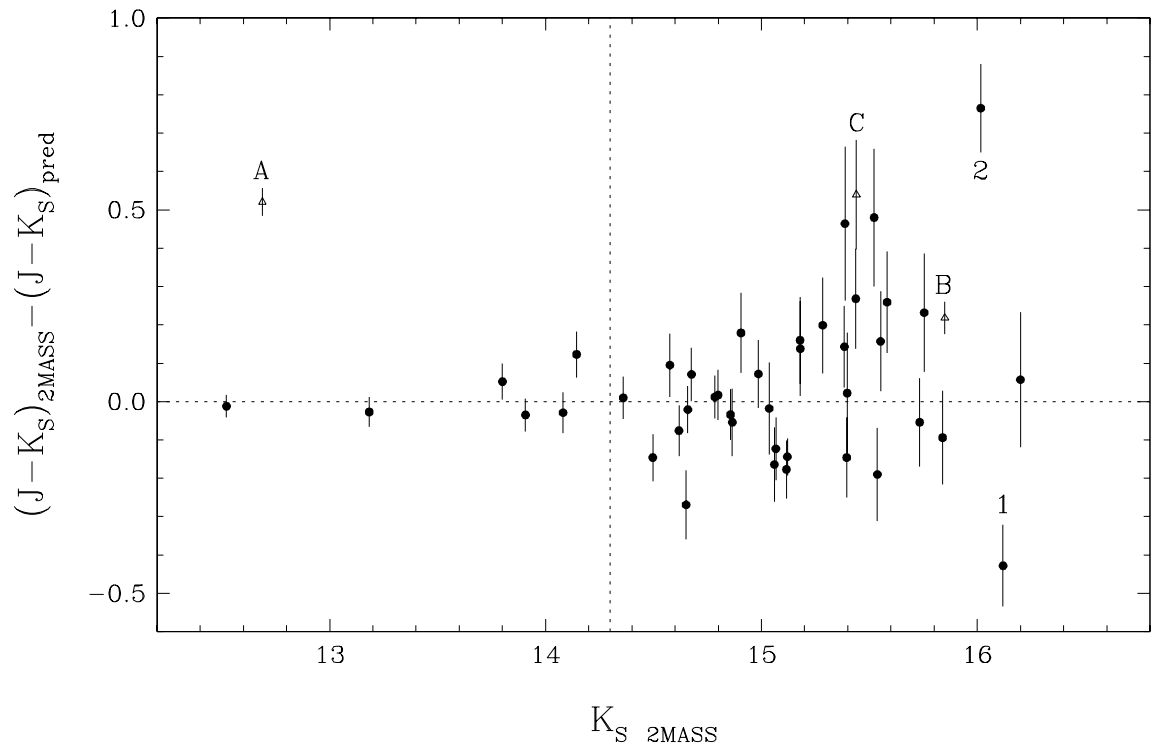
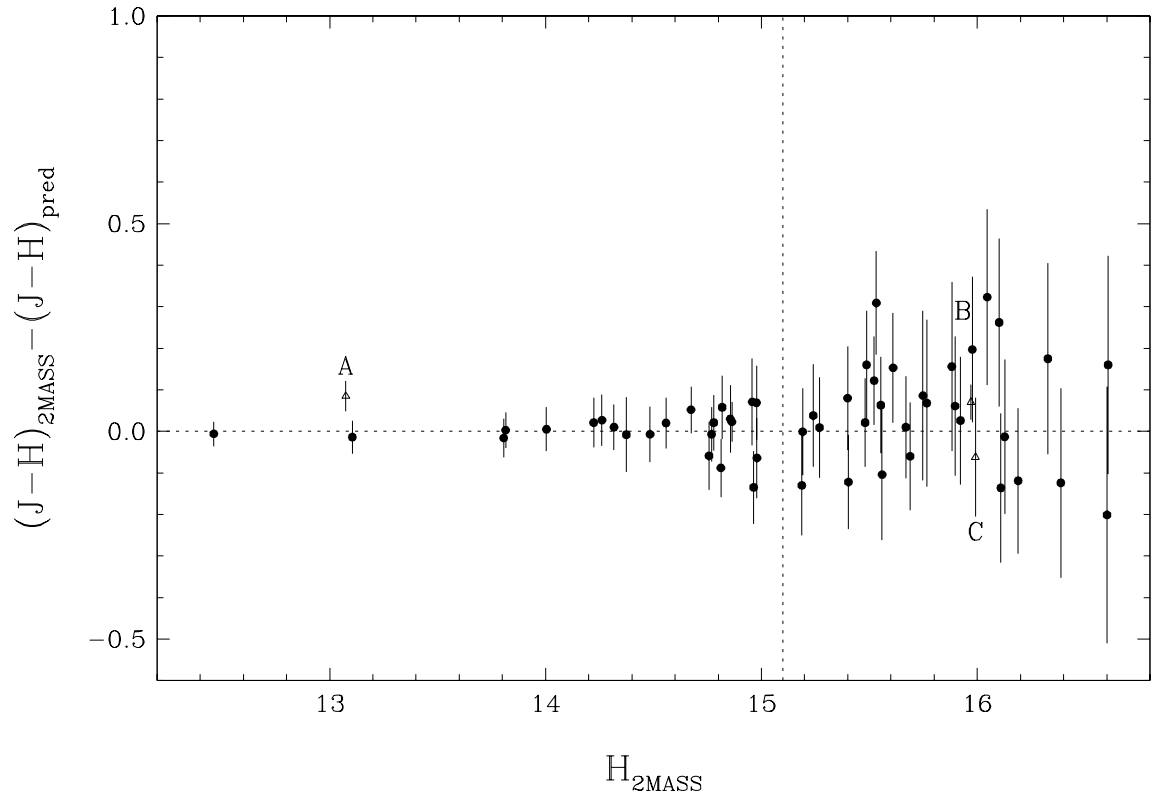


Figure 9